Check for updates

Programmable DNA switches and their applications

Scott G. Harroun, [ID] †[a] Carl Prévost-Tremblay,†[a,b] Dominic Lauzon, [ID] [a]
Arnaud Desrosiers,[a,b] Xiaomeng Wang,[a] Liliana Pedro[a] and
Alexis Vallée-Bélisle [ID] *[a,b]

DNA switches are ideally suited for numerous nanotechnological applications, and increasing efforts are being directed toward their engineering. In this review, we discuss how to engineer these switches starting from the selection of a specific DNA-based recognition element, to its adaptation and optimisation into a switch, with applications ranging from sensing to drug delivery, smart materials, molecular transporters, logic gates and others. We provide many examples showcasing their high programmability and recent advances towards their real life applications. We conclude with a short perspective on this exciting emerging field.

1. Introduction

Through billions of years of evolution, living organisms have developed and perfected nanoscale tools for sensing and adapting to changes in their environment. In order to make decisions, cells rely on protein or nucleic acid switches undergoing structural changes in response to specific inputs. In turn, these structural changes are coupled to a plethora of outputs, ranging from regulation of genes and enzymes to the formation of localised macromolecular complexes and architectures. Because these structure-switching molecules are reversible, and endowed with remarkable affinity, specificity and speed, they can operate continuously in complex surroundings. Such molecular switches are therefore ideally suited for numerous nanotechnological applications, and increasing efforts are being directed toward their engineering.

One superstar molecule in the field of nanotechnology is DNA. Because of its high structural and thermodynamic programmability, its easy synthesis, and possible conjugation to a wide variety of molecules and nanomaterials, DNA has shown an impressive potential to engineer a variety of molecular switches with applications ranging from molecular sensors to therapeutic tools. In addition to its innate ability to recognise and bind its complementary sequence, DNA can also self-assemble into diverse nanostructures that allow it to selectively interact with any class of molecule (Fig. 1-I).[1,2] As a first step

in the creation of a DNA switch, one must select a DNA molecule that specifically recognises a desired input molecule (Fig. 1-I). This recognition element is then transformed into a molecular switch by stabilisation of an alternative conformation (Fig. 1-II and Fig. 2). By adding reporter or other functional moieties, these structure-switching nanodevices can then be engineered to perform a wide range of functions including providing a measurable signal, triggering enzymatic activity, releasing a cargo, or reshaping materials (Fig. 1-III). Finally, numerous strategies can be employed to modulate the dynamic range of DNA switches in order to achieve optimal function within an input concentration range of interest (Fig. 1-IV). These four essential steps of DNA switch design (Fig. 1) have allowed for the successful development of a variety of DNA nanomachines pushing the boundaries of bioanalytical research, and open new possibilities as smart vehicles for controlled drug delivery and drug design. In this review, we summarise the design principles of DNA switches, and highlight the most recent and interesting advances in their applications. We conclude by exposing some of the challenges that this technology must face before realising its full potential.
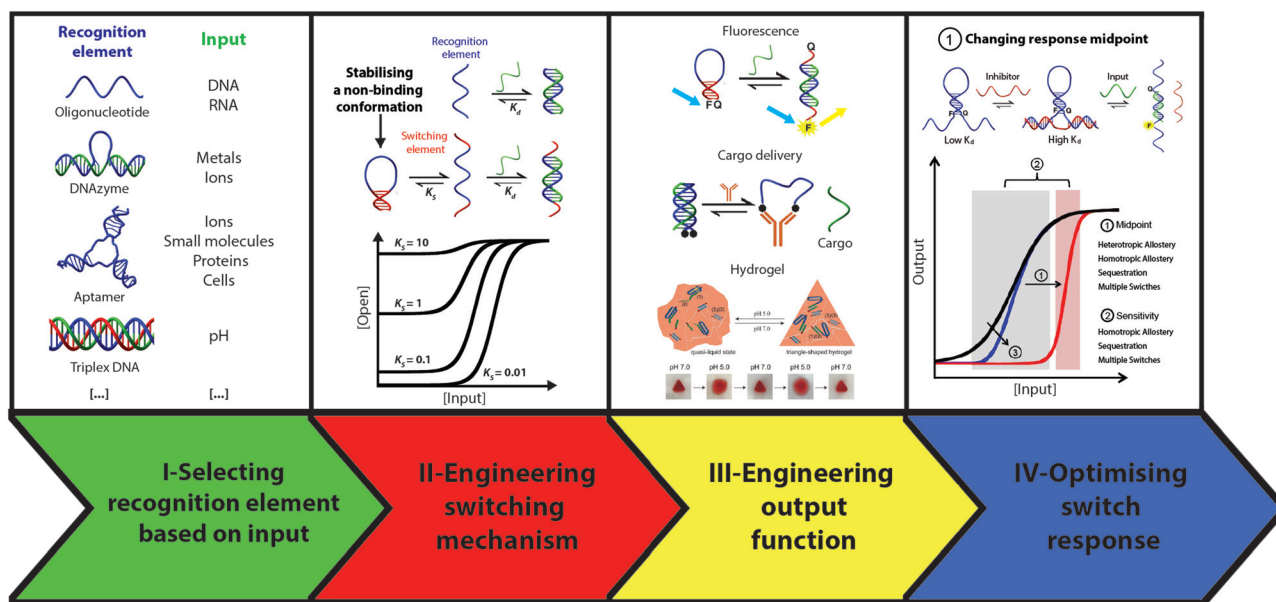
2. DNA switch design

When designing a DNA switch-based system, one must consider all aspects: (1) a recognition element will be selected for its ability to specifically bind a desired input stimulus; (2) a structure-switching mechanism will be designed for its ability to provide an appropriate conformational change for a specific output mechanism; (3) the switch will be adapted for a specific output method; and (4) the switch input/output response must

[a]Laboratory of Biosensors & Nanomachines, Département de Chimie, Université de Montréal, Montréal, Québec H3C 3J7, Canada. E-mail: a.vallee-belisle@umontreal.ca
[b]Département de Biochimie et Médecine Moléculaire, Université de Montréal, Montréal, Québec H3C 3J7, Canada
†These authors contributed equally.

Fig. 1 Essential steps of DNA switch design. (I) DNA nanostructures can act as a specific recognition element for a broad spectrum of input molecules. (II) A selected recognition element can be converted into a structure-switching device by engineering an alternative non-binding conformation. (III) Structure-switching triggered by the input can be used to regulate the activity of diverse functional or reporter moieties. (IV) A number of strategies allow one to rationally modulate the dose–response profile of DNA switches to better suit the needs of diverse applications.

be optimised. These factors are interdependent, and while we discuss them in a linear manner herein, one must consider all four in a comprehensive approach when developing a chemical system based on DNA switches. We also note that while there are a multitude of DNA recognition elements and output methods relevant to the monitoring of nanomachines, this review focuses mostly on switch design and programmability strategies.

2.1 Selecting a DNA recognition element

DNA switches can be triggered by a variety of inputs, ranging from physical phenomena such as temperature, light or current, to chemical stimuli such as protons, metal ions, or other small molecules, and also to much larger nucleic acids
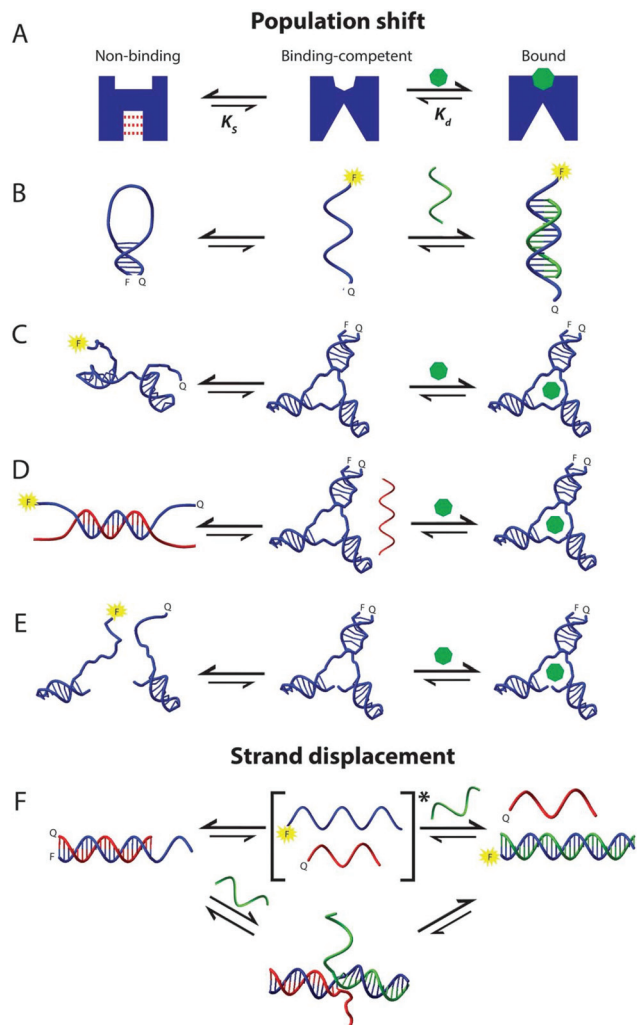
and proteins (Fig. 1-I). The first step of switch design therefore requires selecting the appropriate recognition element for a desired input molecule/signal. DNA structures can be selected for their temperature-sensitive behavior,[3–7] designed to become light-sensitive (*i.e.* by employing photoisomerisable *trans*-azobenzene),[8,9] or can be driven by electrochemical processes by controlling interaction between nucleic acids and metal ions.[10] Specific metal ions can stabilise G-quadruplex secondary structures,[11–14] Hg^{2+} can specifically bind to T:T mismatched base pairs,[15,16] and Ag^+ can stabilise C:C mismatches.[16,17] Cytosine-rich strands can form i-motifs at acidic pH,[18–20] while parallel triplex DNA also requires acidic pH for its formation.[21] Atoms, small organic molecules and proteins (including also bacterial and viral proteins) can be specifically

and Xiaomeng Wang, research agent Liliana Pedro, and Prof. Alexis Vallée-Bélisle.

Professor Vallée-Bélisle and his multidisciplinary group are inspired by nature in developing biotechnologies and nanotechnologies, including biosensors and nanomachines, aimed at making improvements in global health and environmental issues. Current and past research projects in the lab involve the development of steric hindrance-based DNA electrochemical biosensors for rapid detection in whole blood, controlled drug delivery systems, programmable DNA switches for temperature and pH monitoring, and thermodynamic and kinetic studies of complex biochemical mechanisms (e.g. monitoring enzyme kinetics and exploring binding mechanisms using DNA nanotechnology).

Shown from left to right are PhD students Scott G. Harroun, Carl Prévost-Tremblay, Dominic Lauzon, Arnaud Desrosiers

Fig. 2 Engineering switches by creating an alternative non-binding state. (A) Schematic representation of the population-shift mechanism used to create DNA switches. The switch (blue) is in equilibrium between non-binding and binding-competent states (K_S). In the presence of an input (green), this equilibrium is shifted towards the bound state. (B) Creating a non-binding conformation through addition of complementary sequences at the extremities of the recognition element (*e.g.* molecular beacons),[48] (C) through mutations or deletions that destabilise the binding-competent conformation,[49] (D) through addition of a competitor oligonucleotide (red), (E) by splitting the recognition element in two halves, or (F) by employing a strand displacement mechanism. *The intermediate in brackets does not represent the kinetic intermediate (represented below), but it is used to represent the effect of K_d and K_S on the equilibrium between the initial and final states (K_d^{app}), which is independent of the stability of this intermediate state.

recognised by DNA aptamers.[22–26] Aptamers, which are designed through various selection strategies (*e.g.* SELEX),[27,28] are typically sequences with 15–40 nucleotides that fold into complex and specific tertiary folds that enable molecular recognition with any desired targets with high affinity and high specificity.[22–26] DNA aptamers employing modified nucleobases, often referred to as SOMAmers, can also improve affinity and specificity for a desired target.[29,30] Finally,

DNAzymes are nucleic acids known to catalyse enzymatic reactions, ranging from oligonucleotide nicking and ligation to organic synthesis. Besides catalysis, DNAzymes can also be used for signal amplification.[31–35] Multiple recognition elements can be utilized in a single system, such as in bioinspired constitutional dynamic networks (CDNs) to emulate the principles of natural processes.[36,37]

2.2 Engineering switching

The performance of DNA switches (*i.e.* the signal output) is often linked with the magnitude of the conformational change that takes place in the presence of their input molecule. While some DNA structures spontaneously undergo large structural changes upon binding to their input molecule, most DNA structures do not display intrinsic structure-switching activity. To circumvent this limitation, various strategies have been established to implement or enhance binding-induced structure-switching in any DNA recognition element.[38,39] These strategies are generally based on the population-shift model, and involve the creation of an alternative non-binding structure (Fig. 1-II, Fig. 2A).[37,40,41] In order to create an efficient switch, the population-shift model dictates that a binding-competent DNA molecule must be engineered to adopt a low-energy non-binding conformation in the absence of an input. In the presence of an input molecule, binding and stabilisation of the binding-competent conformation triggers structure-switching by shifting the equilibrium toward this state (Fig. 2A).[42] Design and energy prediction of simple DNA secondary structures, and therefore energy differences between two conformations involved in switching, is readily achieved using software like *NUPACK*[43] or *Mfold*.[44] To achieve the assembly of a target secondary structure through a prescribed reaction pathway (*i.e.* a sequence of hybridisation and/or dissociation steps involving defined intermediate structures), a *NUPACK* web application has been recently developed to perform sequence design that minimises off-pathway and crosstalk interactions between the different species generated during all elementary steps.[45] Experimental validation of the switching energy or binding free energy ($\Delta G = -RT \ln K_S$) can be obtained from urea[46] or temperature[47] denaturation curves. Low background and large signal amplitude are generally achieved with a switching equilibrium constant (K_S = [binding-competent]/[non-binding]) lower than 0.1, so that more than 90% of the switch population transitions from the non-binding to the binding-competent state in the presence of an input (Fig. 1-II).[40] However, stabilising the non-binding conformation (reducing K_S) also raises the energetic penalty that binding must overcome in order to hold the switch in the binding-competent conformation. As a result, the concentration of input required to shift the equilibrium from the non-binding to binding-competent state (K_D^{app}) is increased relative to the intrinsic affinity of the recognition element (K_D) following the relationship: $K_D^{app} = K_D[(1 + K_S)/K_S]$ (Fig. 1, panel II).[40] Therefore, the non-binding conformation should not be overstabilised as this leads to switches being unable to respond in a useful range of input concentrations. The lowest

limits of detection are generally achieved around a K_S of 1, which yields a maximum signal gain of 50% (since 50% of the switch is already in the "on" conformation in the absence of input), while only decreasing the observed affinity of the recognition element, K_D^{app}, by 2-fold.

Numerous strategies have been explored to stabilise an alternative non-binding structure in an arbitrary DNA recognition motif (Fig. 2). A first approach is to add complementary oligonucleotide sequences at both extremities of the recognition element to constrain its structure in a non-binding geometry. This strategy is employed to design molecular beacons,[48] where the double-stranded stem bends and shapes the recognition sequence in the form of a loop, which differs from the linear helix conformation that it adopts when binding its complementary strand (Fig. 2B). A second approach to create an alternative non-binding structure is to introduce mutations (or deletions) that destabilise the secondary structure of the binding-competent conformation (Fig. 2C).[49] The unfolded recognition sequence still transiently samples its native binding-competent state, and the equilibrium shifts back towards this native state in the presence of the ligand. If the structure of the bound complex is known, the mutations should be introduced far from the binding site to avoid alteration of the binding specificity. A third strategy employs a complementary DNA sequence, either appended to the recognition element or supplied as a separate strand, that is able to occupy the binding site and compete with input binding (Fig. 2D).[50,51] It is also possible to engineer switches that undergo changes in oligomerisation state by splitting the recognition motif in two halves that come together upon input binding (Fig. 2E).[39] These strategies based on the population shift mechanism have been widely employed to engineer structure-switching in all types of DNA recognition elements (e.g. aptamers, molecular beacons, G-quadruplexes, etc.) and are thus applicable for inputs of various natures. The strand displacement mechanism is also commonly used to create DNA switches. Here, the alternative conformation corresponds to a DNA duplex bearing a single-stranded terminal anchor, called a toehold domain, that can hybridise to a portion of the input DNA strand. This toehold duplex can undergo a strand exchange process in the presence of an input DNA strand complementary to both the toehold and duplex regions of the recognition strand (Fig. 2F).[52] While the transition from one duplex to another must be initiated by an invading DNA molecule, it can be made responsive to the presence of other classes of input molecules. Strand displacement can be triggered by proteins or small molecules using aptamer-bound toeholds,[53,54] by metals and ions using bimolecular G-quadruplexes,[55] or by pH changes using triplex-forming sequences.[56] Strand displacement can also be made responsive to combinations of two input DNA strands that cooperatively invade the initial duplex region, making it possible to design logic gates and establish threshold responses in toehold-based DNA devices.[57] Moreover, strand displacement across three-way junctions can be used to replace the irreversible phosphate linkage between the toehold and duplex region by a reversible base pair linkage. Such an associative toehold mechanism makes it possible to reversibly modify a toehold sequence and change the switch's input on-the-fly.[58]

2.3 Output

A variety of methods exist for measuring output signals to record the structural changes of DNA switches. In fact, there are so many approaches available to researchers that Deng et al. have recently numbered more than 100 articles detailing output mechanisms for structure-switching thrombin-binding aptamers.[26] The focus of the present review is not to provide an exhaustive list of all known output methods, but rather to provide a general overview of relevant programmable DNA switch designs for various applications. Switch engineering is intrinsically linked to the selected output mechanism. For example, a change in distance of several nanometers may be desirable for fluorescence spectroscopy relying on Förster resonance energy transfer (FRET) between a fluorophore/quencher pair,[59] for surface-enhanced Raman spectroscopy (SERS) on gold or silver nanoparticles,[60] or for change in electron-transfer efficiency in electrochemical analysis.[61] On the other hand, DNAzymes may only require a small (<0.5 nm) structural variation to activate or inactivate their catalytic activity (i.e. G-quadruplex).[62]

Electrochemical analysis consists of a family of techniques for measuring the structural changes of DNA switches.[63,64] Electrochemical methods, such as cyclic voltammetry (CV) or squarewave voltammetry (SWV) have the advantages of simplicity, rapidity, low cost, high sensitivity and the ability to be used with a portable system in complex media such as whole blood.[65] Typically, these approaches involve immobilisation of the DNA switch on an electrode surface, often gold, via a Au–S bond. Covalently-labelled reporters, such as methylene blue or ferrocene, allow for the measurement of structural changes via redox reactions, wherein the reporter is often brought closer (signal-on) or further away (signal-off) from the surface after the target binding event.[61] Other systems involve intercalation of a ligand, such as methylene blue or daunomycin, into the duplex DNA structure. Redox signal from ions such as $[Fe(CN)_6]^{3-/4-}$ or $[Ru(NH_3)_6]^{3+/2+}$ can be used to determine DNA hybridisation or the amount of DNA on an electrode surface.[66] Alternatively, without attachment to the surface, homogeneous electrochemical assays based on exonuclease-assisted degradation of DNA in the presence of a target can increase electrochemical signal based on enhanced diffusivity of methylene blue to the electrode surface.[67–69] Furthermore, enzyme-free homogeneous electrochemical assays have also been developed.[70,71] Catalytic labels, such as enzymes and catalytic nanoparticles, can also be used for techniques such as electrocatalytic amplification (ECA) for biosensing of nucleic acids.[72]

Another commonly used switch output is fluorescence spectroscopy, typically involving FRET. Fluorescence has the advantages of high sensitivity, high efficiency, and simple handling.[73–75] Typically, covalently attached organic fluorophores are employed, but other fluorescent labels exist as well, such as metal nanoclusters.[76] Among the simplest and most

widely used forms of DNA switches for bioanalytical applications is the molecular beacon, a stem-loop switch that maintains a fluorophore and a quencher located at its extremities next to each other (low fluorescence). Binding of a complementary DNA (cDNA) to the loop sequence triggers stem opening, due to the stiffness of double-stranded DNA (dsDNA), thus separating the fluorophore/quencher pair, and giving rise to a large fluorescent signal. Conformational changes of DNA switches can be used to control adsorption onto graphene oxide and related materials, which can quench fluorescence, and is useful for optical biosensors.[77–79] Considering the higher cost associated with covalently attached fluorescent labels, label-free fluorescence-based techniques also exist, such as using DNA intercalation of fluorescent dyes.[73] Other popular output mechanisms include chemiluminescence and bioluminescence, which differ from fluorescence since the excitation energy comes from a chemical reaction instead of a light source.[73] Switching mechanisms and/or hybridisation can also be detected using electrochemical plasmonic sensing systems[80] and by SERS.[81–83] Colourimetric methods are another means of switch output, for which a change in the colour of gold nanoparticles in the dispersion state *versus* their aggregated state is observed; typically from red to blue.[73]

Several enzyme-assisted approaches allow for signal enhancement in the aforementioned output methods. For example, Exonuclease I (Exo I) digests only ssDNA, whereas Exonuclease III (Exo III) is specific for dsDNA.[84] Conformational changes resulting from target binding can thus take advantage of these specific enzymes. DNAzymes, which are nucleic acids possessing catalytic activity toward specific substrates, can also be used for signal amplification.[85] The hybridisation chain reaction (HCR) allows for signal amplification based on polymerisation of DNA, thus allowing for increased output signal.[86] Rolling circle amplification (RCA) uses nucleic acid polymerases to generate long ssDNA/RNA from a primer DNA annealed to a circular DNA. By generating multiple repeat units, signal can thus be amplified.[87]

In summary, DNA switches are designed to perform a mechanical motion in response to a specific input, and this motion can be detected by an appropriate output method. In addition, this switching motion can be used in mechanical applications such as DNA logic gates and DNA walkers, as well as to introduce macroscale changes *via* conformational changes at the nanoscale, as is seen with shape-changing DNA hydrogels and colour-changing aggregation of nanoparticles. With the specific requirements of the desired or available output method in mind, the only limitation of designing such nanosystems is one's imagination and creativity.
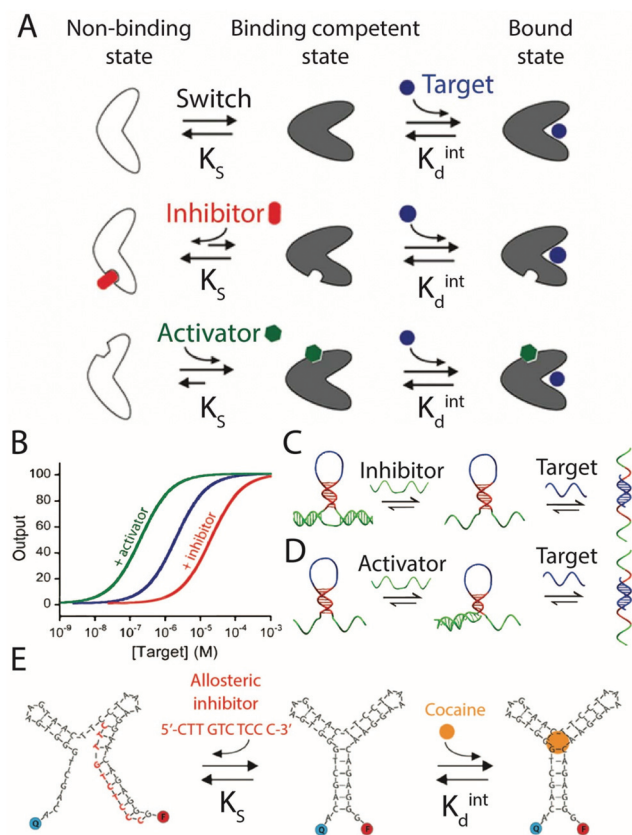
2.4 Optimising switch response

Simply turning a DNA recognition element into a functional switch is often not sufficient to obtain an efficient switch. This is because the dose–response curve of a switch typically requires optimisation to obtain a relevant dynamic range.[88] The dose–response curve profile of a switch can be described with two simple parameters, namely, (1) the midpoint, and (2)

the sensitivity (Fig. 1-IV).[40,89] The midpoint refers to the amount of input that is necessary to obtain 50% of the output signal. This term is generally referred to as the observed dissociation constant K_d^{Obs}, or sometimes just K_d, and represents the inflection point of the sigmoidal dose–response curve.[40,90] The sensitivity, which is defined as the change of output signal over the input concentration window at which this change happens, can be assessed by the ratio of the input concentrations yielding 90% and 10% output signal ($I_{90\%}/I_{10\%}$)[91,92] and by the Hill factor (n_H).[93] A traditional dose–response curve shows an $I_{90\%}/I_{10\%}$ value of 81 or a n_H of 1. High sensitivity corresponds to lowering the input concentration ratio ($I_{90\%}/I_{10\%}$ < 81) or increasing the Hill factor (n_H > 1). The opposite ($I_{90\%}/I_{10\%}$ > 81, n_H < 1) is observed for a less sensitive dose–response curve. The simplest approach to modulate the midpoint of the response has been discussed above in relation to the population-shift model (section 2.2), and involves the stabilisation of an alternative non-binding conformation to shift the midpoint to higher input concentrations. Here, we describe other strategies used to program the two parameters of switch response in order to optimise the performance of DNA devices for a specific application.

2.4.1 Allostery. Nature has developed strategies to tune the affinity of natural switches. One of these is heterotropic allostery, which uses the binding energy of a first effector molecule to alter the conformation and affinity of a distal binding site for a different ligand (Fig. 3A).[94–98] The response at this second site can either be favoured (activation) or disfavoured (inhibition). To demonstrate that the midpoint of a DNA switch response can be programmed using allosteric effectors, Ricci *et al.* designed a simple stem-loop switch (molecular beacon) with two tails acting as an allosteric binding site.[90] To create an inhibited molecular beacon, they used a long DNA strand that binds both tails simultaneously (Fig. 3C). This bridges the junction between the tails, and stabilises the non-binding state by keeping the stem closed. Consequently, the affinity of the target towards the molecular beacon is reduced, and the midpoint of the dose–response curve shifts to a higher concentration (Fig. 3B). In an opposite scenario, they designed a DNA strand that binds to one of the tails, and partially invades the stem of the molecular beacon (Fig. 3D). This destabilises the non-binding state, thus increasing the affinity of the target towards the molecular beacon, shifting the midpoint to a lower input concentration (Fig. 3B).
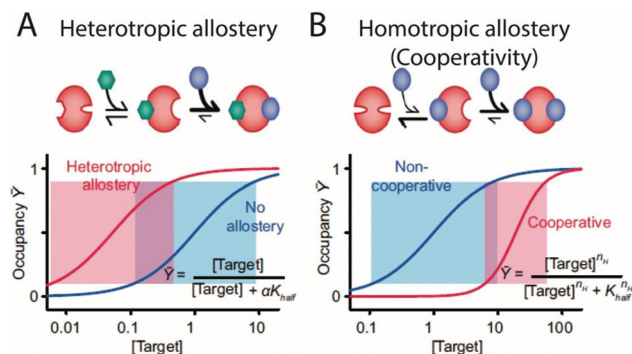
This heterotropic allosteric mechanism was further adapted by Porchetta *et al.* to create allosterically-controlled aptamers (Fig. 3E) and metal ion switches (section 3.2.3., Fig. 15).[99,100] First, they created three inhibitor DNA strands of different lengths for the original cocaine aptamer.[49] In doing so, the dissociation constant of cocaine was shifted from the original value of 0.5 μM to 2.9, 19 or 235 μM with inhibitors of increasing length (10 to 14 nucleotides). The authors found that the usage of allosteric effectors provides a more predictable approach to alter the input affinity compared to the mutagenesis strategy, since random or structure-based mutations are likely to modify the specificity of molecular recognition. The

Fig. 3 Tuning switch response using allosteric inhibitors and activators. (A) A three-state model description of allosteric switches. (B) Inhibition leads to a higher midpoint, and activation leads to a lower midpoint of the dose–response curve (C) The inhibitor strand stabilises the non-binding state by linking both tails. (D) The activator destabilises the non-binding state by invading the stem of the molecular beacon. (E) The inhibitor strand stabilises the unfolded state of the cocaine aptamer. Panels A–D are adapted with permission from ref. 90. Copyright 2012 American Chemical Society. Panel E is adapted with permission from ref. 99. Copyright 2012 American Chemical Society.

usage of DNA strands acting as activators or inhibitors thus provides a rational means by which the response of DNA switches can be finely-tuned through the population-shift model.

While heterotropic allostery provides an efficient way of shifting the midpoint of a dose–response curve to lower or higher concentrations, it cannot affect sensitivity (Fig. 4A). In contrast, homotropic allostery differs from heterotropic allostery by the fact that the effector molecule is the same as the ligand (also referred to as "cooperativity").[91] This provides a change in both the midpoint of the curve and its shape to a more sensitive (positive cooperativity) or less sensitive (negative cooperativity) profile (Fig. 4B).[91] One of the most characterised biological switches that employs homotropic allostery is hemoglobin. Oxygen binding to one of the four heme domains of hemoglobin increases the affinity of oxygen for the three remaining binding sites, resulting in highly sensitive loading and release of oxygen (n_H = 1.7–3.2).[101] This sensitive

Fig. 4 Tuning the dynamic range of switches using heterotropic and homotropic allostery mechanisms. (A) Heterotropic allostery provides a way to fine-tune the midpoint of the dose–response curve (B) homotropic allostery is used to change the sensitivity of the curve as well as its midpoint. Adapted with permission from ref. 91. Published in 2014 by the National Academy of Sciences.

or cooperative behavior enables oxygen delivery from the lungs to tissues with only a ~3-fold dynamic range, which contrasts with the usual 81-fold dynamic range of a non-cooperative switch.[102] Inspired by the hemoglobin delivery system, many groups have used homotropic allostery to design high sensitivity DNA switches for various applications such as drug delivery systems,[102,103] biosensors,[90,99] metal-ion-triggered molecular switches,[100] nanoactuators[104] and logic gates.[105–107]

To demonstrate the application of homotropic allostery in the field of DNA switches, Simon *et al.* designed a simple stem-loop that contains two identical binding sites.[92] They used two variations of this design; the first one being asymmetrical, and having one binding site in the loop, and another partially inside the stem and partially exposed as a tail (Fig. 5A), and the second design being symmetrical with both binding sites corresponding to half of the loop (Fig. 5B). Both homotropic designs showed higher sensitivity compared to the heterotropic and the single binding site designs. In addition, Simon *et al.* also introduced a generalisable strategy based on
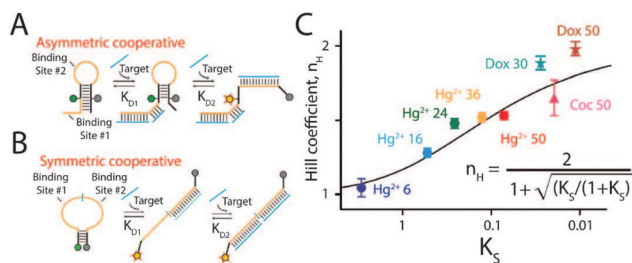
Fig. 5 Creating cooperative switches through homotropic allostery. (A) A non-symmetrical cooperative design; (B) a symmetrical cooperative design (C) the sensitivity of the dose–response curve for different molecular beacons is directly related to the conformational equilibrium (K_S) between the low affinity and high affinity states. Panels A and B adapted with permission from ref. 92. Copyright 2014 Wiley-VCH. Panel C adapted with permission from ref. 91. Published in 2014 by the National Academy of Sciences.

disorder-to-order transitions, enabling the implementation of homotropic allostery in various types of DNA switches.[91] The switch consists of two tandem recognition elements split in halves that are linked by a long destabilising unstructured loop. The first binding event requires the energetically unfavourable closing of this loop, reducing its affinity relative to that of the second binding event that occurs at a preformed site. They showed that by increasing the number of bases in the loop, thus increasing the entropic cost of closing this linker (K_S), a gain in sensitivity is achieved (Fig. 5C). This design strategy also allowed for the rational introduction of cooperativity in three unrelated DNA switches (Hg^{2+}, doxorubicin and cocaine), thus demonstrating the generality of this approach.

2.4.2.   Sequestration mechanism. Using homotropic allostery, the maximal cooperativity that can be achieved by a switch increases proportionally with the number of ligands.[93] In terms of the Hill factor, having two binding sites on the switch provides an upper limit of $n_H = 2$ (corresponding to a switch yielding a change from 10% to 90% of its maximal response on a 9-fold change of ligand concentration). This leads to the problem of homotropic allostery, where higher-order sensitivity ($n_H \geq 2$, meaning that less than 9-fold is necessary to reach change in output signal from 10% to 90%) can only be achieved by significantly increasing the number of binding sites, which can be challenging for the design of the switch.[108,109] To overcome this problem, nature takes advantage of the sequestration mechanism to achieve ultrasensitivity ($n_H > 2$) in regulatory networks, signaling pathways, inhibition mechanisms, and to achieve a rapid response to biological inputs.[108,110] This mechanism uses a high affinity receptor as a "depletant" to sequester all the ligands (or inputs) into an inactive complex much like a "sink" that prevents the accumulation of free and active ligand inside the system. When the ligand is added to the system, it first binds to the depletant of higher affinity until the depletant becomes saturated (*i.e.* the sink is filled). As the total ligand concentration exceeds the depletant concentration, the ligand starts to bind and activate the switch in a threshold response that can be much more cooperative than homotropic allostery.[108,109] Mathematical and computational modeling of the sequestration mechanism by Buchler and Louis has shown that a key parameter controlling ultrasensitivity is the stoichiometric binding parameter defined as the ratio of the total depletant concentration over the depletant affinity (B_T/K_d).[109] This model revealed that sequestration of the input can yield incredibly sensitive responses. For example, when the ratio B_T/K_d is set at 10^4, a Hill factor of 21.6 is obtained, corresponding to a switch producing a change from 10% to 90% of its maximum response over a 1.22-fold change of input concentration.[109] This Hill factor is enormous in comparison with the maximum of 2 that can be attained by a homotropic allosteric switch with two ligands.

Encouraged by the programmability of this nature-inspired system, Kang *et al.* designed a sequestration-based DNA switch using a depletant molecular beacon and a probe molecular beacon (Fig. 6A).[108] The depletant molecular beacon was designed with a higher affinity for the target DNA than that of the probe molecular beacon for the same target ($K_d^{dep} < K_d^{probe}$). By simply changing the stability of the molecular beacon's stems (K_S), they demonstrated experimentally that sensitivity (Hill coefficient) increases proportionally to the ratio of K_d^{probe}/K_d^{dep}. They further demonstrated that an increase in sensitivity is obtained by increasing the depletant concentration, and that ultrasensitivity is only obtained when the depletant concentration exceeds the probe dissociation constant ([dep]/$K_d^{probe} > 1$). In fact, improved sensitivity requires a concentration of depletant high enough to sequester the target in a range of concentrations where binding to the probe would normally occur (around or above K_d^{probe}). Because of this, a gain in sensitivity is achieved at the cost of increasing the smallest concentration of input that can be detected (higher detection limit), thus shifting the midpoint of the dose–response curve to a higher concentration (Fig. 6B). Additionally, the 81-fold dynamic range of a molecular beacon is compressed into a dynamic range of only 1.5-fold ($n_H = 9.4$). A similar approach was recently used for an electrochemical biosensor.[111] By adding both signaling and depletant strands at the surface of an electrode, and designing them such that the depletant strand displayed higher affinity towards its target, Kang *et al.* achieved a pseudo-Hill factor ranging from 1 (without depletant) to 2.3 (with a ratio [dep]/[target] = 50) without significantly affecting the output signal by saturating the electrode with a huge amount of depletant strand ([dep]/[target] > 50). In light of these studies, the sequestration mechanism represents a straightforward means to improve sensitivity, as it requires only a depletant of higher affinity to bind the target.
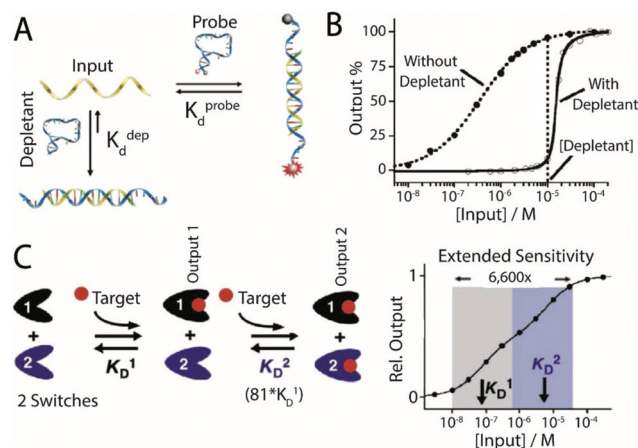
Fig. 6 Narrowing and extending the dynamic range of switches (A) DNA approach illustrating the sequestration mechanism. (B) In the presence of depletant, sharp dose−response curves are achieved at a threshold concentration corresponding to the saturation point of the depletant. (C) Two or more switches can be used to enlarge the sensitivity of the relative output signal. Panels A and B are adapted from ref. 108. Published in 2011 by Public Library of Science. Panel C is adapted with permission from ref. 88. Copyright 2011 American Chemical Society.

2.4.3. Mixture of switches. In contrast to the sequestration and allosteric mechanisms that produce narrower dynamic ranges, a strategy to extend the dynamic range of a switch is to combine multiple switches with different midpoints.[88] When an optimal ratio of all switches is used, the dynamic range relative to a single DNA switch can be extended to more than the classic two orders of magnitude (81-fold) of a regular dose–response curve (Fig. 6C).[88,99,100] This was achieved by Porchetta *et al.* by combining two inhibitors of the cocaine aptamer of different lengths.[99] With this strategy, they obtained a dynamic range of 50 000-fold with a good log-linearity. They even reached a higher dynamic range of 330 000-fold when combining four variants of the cocaine aptamer that have different affinities for cocaine. However, when only using inhibitors or switch variants of reduced affinity, this method is limited to shifting the midpoint of the dose–response curve to higher input concentrations. This can be problematic if one wants to extend the dynamic range of a switch around its natural midpoint.

To overcome this, Porchetta *et al.* used a combination of activators and inhibitors to extend the dynamic range in a symmetrical fashion.[100] While the activator extends the dynamic range to lower concentrations relative to the original midpoint, the inhibitor extends it symmetrically towards higher concentrations. Using a Hg^{2+}-specific molecular beacon combined with two DNA strands serving as an activator and an inhibitor, the authors were able to extend the dynamic range to 333-fold while maintaining the midpoint of the curve around 16 μM; near the K_d of the original Hg^{2+} molecular beacon. Lastly, Kang *et al.* applied this strategy to extend the dynamic range of an electrochemical biosensor by attaching two molecular beacons with different affinities at the surface of a gold electrode, and increased the dynamic range from 81-fold to 1000-fold.[111] One must keep in mind that a detailed characterisation of each switch, activator or inhibitor in terms of their individual input-output response is a prerequisite when using any of the above-mentioned strategies.[99,100,111] This information, combined with simulations using the population-shift mechanism, will allow for optimal switch ratio determination.[40,88]

3. Biosensing applications

DNA switches engineered based on the principles discussed in the preceding section can be used for a variety of biosensing applications. First, we discuss their use for detection of physical parameters including temperature and light. Then, we discuss using these switches for the detection of chemical species relevant to health and environmental monitoring, ranging from protons and heavy metal ions, to small molecules such as cocaine and pesticides, and up to larger biomolecules such as nucleic acids and proteins.

3.1. Detecting physical parameters

3.1.1. Temperature. Detection of temperature at the nanoscale may be useful for various applications, including monitoring cellular processes, detection of pathogenic cells with higher temperatures, and understanding the mechanism of photothermal therapy. For this purpose, Ke *et al.* have developed a fluorescent L-DNA nanothermometer that switches from a folded structure to an unfolded conformation as temperature increases.[3] This nanothermometer adopts a stem-loop structure that keeps a fluorophore and quencher pair in close proximity, and undergoes an unfolding transition upon increasing the temperature, which results in the fluorophore moving away from the quencher and a corresponding rise in signal intensity over a 25–30 °C temperature range. The L-DNA sequence prevents recognition by natural nucleic acids or by single-stranded D-DNA binding protein (SSB), as well as enzymatic digestion. These robust nanothermometers were used for monitoring temperature changes in three types of cancer cells, as well as during photothermal therapy, but their dynamic ranges lack programmability.[3] Jonstrup *et al.* then showed how the melting temperature (T_m) of DNA nanothermometers can be simply programmed by modifying the base composition of the stem and the loop components (Fig. 7A).[4] Ebrahimi *et al.* attached similar DNA nanothermometers to gold nanoparticles (13 nm diameter), which serve as both carriers as well as universal quenchers for the fluorescent tags *via* the FRET and nanometal surface energy transfer (NSET) mechanisms. Using this system, they demonstrated multiplexed sensing by attaching two or three different nanothermometers with varying T_m values, with each containing different fluorescent tags.[5]

One limitation of these nanothermometers is that their fixed dynamic range typically leads to several drawbacks. This includes the high cost (money and time) for synthesising fluorophore-labeled DNA sequences with the correct dynamic range, a weak signal gain, and a fixed dynamic range. Using a bio-inspired allosteric regulation mechanism, Gareau *et al.* developed DNA nanothermometers with programmable temperature windows (Fig. 7B).[6] Stem-loops with overhang sequences allow for addition of inexpensive unlabelled DNA stabilisers of varying lengths, which can be used to tune their T_m (Fig. 7B). This study also reported ultrasensitive DNA thermoswitches made from more complex DNA folds, such as a triplex clamp structure in which a fluorophore/quencher-labelled clamp interacts with a second DNA strand through Watson–Crick and Hoogsteen base pairing (Fig. 7C). These ultrasensitive nanothermometers can sense temperature changes as low as ±0.05 °C. Finally, combining six dual-labelled stem-loops (or a combination of stabilisers of varying lengths) allowed for sensing over a 48 °C range (Fig. 7D).

Most recently, Wu *et al.* reported fluorescent nanothermometers based on short unstructured single-stranded DNA (ssDNA) that uncoil at higher temperatures.[7] Optimal DNA sequences were determined using molecular dynamics (MD) simulations. The wide linear dynamic range of these switches (0–100 °C) was unaffected by increasing concentrations of the DNA itself, as well as by Na^+, K^+, PBS, glycerol and bovine serum albumin (BSA). In addition to measurement of the internal temperature of cells, these ssDNA nanotherm-
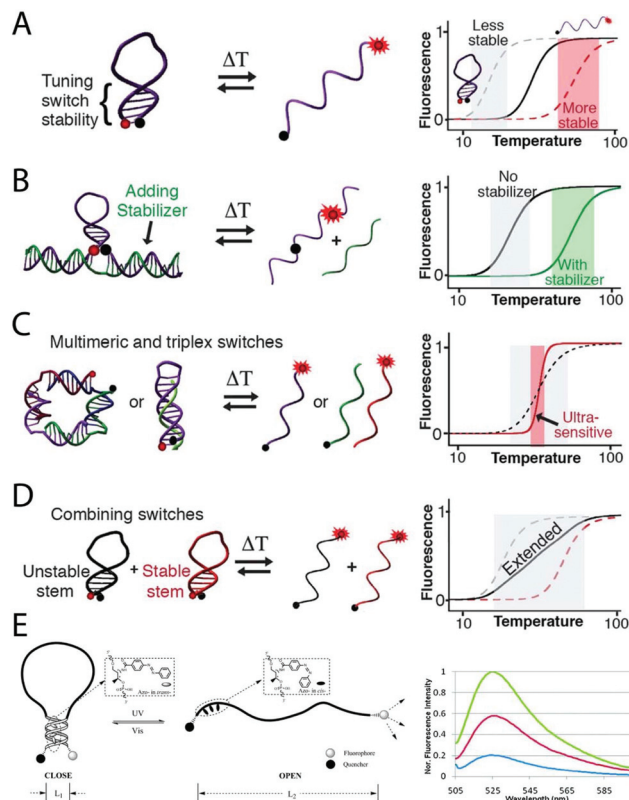
Fig. 7 Bioinspired programmable DNA-based nanothermometers for sensing of temperature and light at the nanoscale. (A) Tuning the dynamic temperature range by modifying the stability of the stem. (B) Tuning the dynamic range by adding an unlabeled allosteric DNA stabiliser strand. (C) Enhancing the sensitivity by engineering multimeric switches. (D) Extending the dynamic range by combining multiple switches or stabilisers. (E) Photo-sensitive DNA switch based on azobenzene isomerisation. The blue curve represents the fluorescence spectra of the switch under visible light, the green curve in presence of 5× of cDNA (duplex conformation), and the red curve under UV light. Panels A–D are adapted with permission from ref. 6. Copyright 2016 American Chemical Society. Panel E is adapted with permission from ref. 112. Copyright 2009 American Chemical Society.

ometers were also used for fluorescent thermoimaging of tumor tissue during microwave hyperthermal treatment.[7]

3.1.2. Light. Light-triggered DNA switches based on photoisomerisable azobenzene have also been developed (Fig. 7E). *trans*-Azobenzene can stabilise duplex DNA structures *via* π–π interactions. Exposure to ultraviolet (UV) light results in its isomerisation to *cis*-azobenzene, which does not stabilise duplex DNA. The system can be made reversible *via* reverse isomerisation to *trans*-azobenzene *via* exposure to visible light. Kang *et al.* have integrated this system into a fluorescently labelled hairpin DNA structure to yield a reversible light-driven molecular motor.[112] Elsewhere, Wang *et al.* have integrated an azobenzene derivative with DNA to control the formation of a G-quadruplex secondary structure *via* light irradiation.[113] For a more broad discussion of the design and applications of photosensitive DNA switches, the reader is directed to these articles.[114,115]

3.2. Detecting chemical inputs

Since the development of molecular beacons in 1996 by Kramer and Tyagi,[48] arguably the most useful DNA-switch developed to date (employed in most hospitals for the real-time detection of DNA amplicons in PCR diagnostics applications), many DNA switches have been adapted for the rapid detection of a wide range of complex molecular inputs. Over the last few years, many reviews[23,26,39,51,63,116–128] have highlighted the recent developments of such switches. In this section, we focus our attention towards recent DNA switches for *in vivo* as well as for health and environmental monitoring applications.

3.2.1. pH. Idili, *et al.* have developed programmable pH-sensitive switches with triggered opening/closing over specific pH ranges (Fig. 8).[129] These rely on a triplex structure stabilised by Watson–Crick and parallel Hoogsteen interactions. While the Watson–Crick interactions are effectively insensitive to pH, the Hoogsteen interactions show strong and programmable pH-dependence. For example, CG·C$^+$ parallel triplets can only form when the cytosine in the third strand is protonated (pK_a ~ 6), and the TA·T triplets are destabilised upon deprotonation at higher pH (pK_a ~ 10). When adding terminal fluorophore and internal quencher conjugations, it is possible to monitor the pH-induced triplex-to-duplex transition. Although each pH-sensitive nanoswitch has a typical dynamic range of about ~1.8 pH units, the range can be further extended to ~4.0 or ~5.5 pH units by means of a combination of two or three pH-sensitive nanoswitches, respectively.[129]
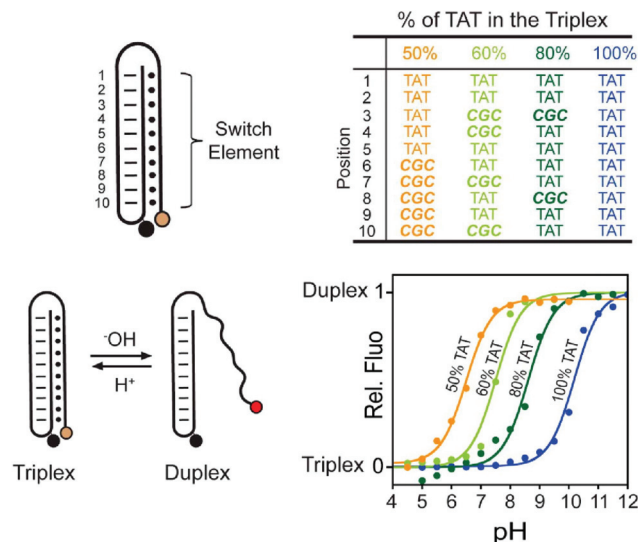
Fig. 8 Programmable pH nanoswitches. The pH-sensitive triplex interactions are tuned by varying the CGC *vs.* TAT content in the switch element. For example, a switch with 100% TAT triplets will open at basic pH (blue), while increasing the CGC content will shift the pH-sensitive range to more acidic pH values (green, light green, orange). Reprinted with permission from ref. 129. Copyright 2014 American Chemical Society.

In order to expand the pH-sensing range *versus* previous designs, Halder *et al.* developed a series of pH-sensitive DNA switches based on the i-motif structure.[130] Crucially, the addition of 5-bromocytosine or 5-methylcytosine modifications allows for expansion into the acidic and mildly basic pH ranges, respectively. One of the designs showing a wide pH regime (pH 5.3–7.5) and a large signal gain is attributed to the introduction of substituents on the cytosines possibly distorting the i-motif structure so that the fluorophores are positioned optimally for FRET.[130] Narayanaswamy *et al.* reported highly reversible DNA switches for pH sensing in synthetic vesicles and HeLa cells based on the molecular beacon and A-motif structures. Under physiological conditions (pH = 7) the switch is in the closed-state hairpin-like structure wherein the close proximity of Cy3 and Cy5 enables efficient FRET. Upon introduction of acidic conditions, the adenines are then protonated at the N1 (AH^+) position, thus leading to the formation of the open-state A-motif *via* reverse Hoogsteen [AH^+–H^+A] hydrogen bonding interactions. Further stabilisation is achieved *via* electrostatic interaction of the positively charged N1 atom and the phosphate backbone. The probe works over the range of 3–7 pH units, and remains sensitive to small changes in pH of 0.2–0.4 units.[131]

3.2.2. Nucleic acids. In recent years, specific microRNA (miRNA) and messenger RNA (mRNA) molecules have been identified as biomarkers for diagnosis of various diseases. Although molecular beacons can be used to detect miRNA/mRNA *in vivo*, they have also been found to be sensitive to enzymatic degradation. To circumvent this limitation, He *et al.* have developed a DNA tetrahedron nanotweezer (DTNT) for ratiometric detection of tumor-related mRNA (Fig. 9).[132] In the absence of target mRNA, the donor and acceptor fluorophores are separated (off-state; low FRET). However, in the presence of a specific mRNA sequence, binding of the target brings the DTNT into the closed state (on-state), thus bringing the fluorophores into close proximity (high FRET). One main advantage of this switch design is its resistance to false-positive signals, as no change in signal is observed upon switch degradation (*i.e.* there is no FRET between the donor/acceptor fluorophores for both the off-state and the degraded-state). Additionally, the DTNT probe exhibited no cytotoxicity, and could be used for real-time intracellular imaging of mRNAs in living cells, including discrimination of higher or lower mRNA signals for cells treated with β-estradiol or tamoxifen, respectively.[132] Other tetrahedron-based probes for mRNA have also been reported, such as a previous nature-inspired design reported by Tay *et al.* that incorporated a molecular beacon sensing unit outside the tetrahedron which could be used to monitor mRNA in living cells.[133] Zhou *et al.* have designed a multicolour-encoded DNA tetrahedron for multiplexed detection of intracellular miRNAs, a so-called "DNA TetrNano". It can detect two specific miRNAs, each by a separate fluorophore/quencher pair. In the off-state, the fluorophore/quencher pairs are in close proximity. In the presence of one or two specific miRNA target sequence(s), these hybridise to the switch, unfold the hairpin structures, and lead to an increase in fluo-
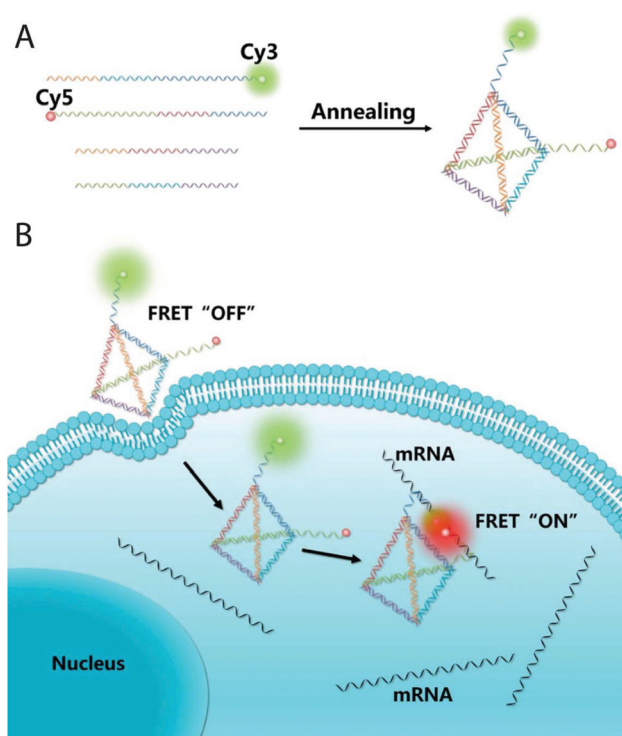

Fig. 9 DNA tetrahedron nanotweezer. (A) Assembly and (B) mechanism of the degradation-resistant DNA tetrahedron nanotweezer (DTNT) nanoprobe used for tumor-related mRNA detection in living cells *via* a FRET "OFF" to FRET "ON" strategy. Adapted with permission from ref. 132. Copyright 2017 American Chemical Society.

rescence signal for either or both fluorophores. In the presence of cell lysates, a standard molecular beacon was degraded significantly over time, whereas the TetrNano showed much less signal change over a longer time period. In addition to resistance to nuclease digestion, this system showed high cell viability, and could thus be used for intracellular miRNA imaging.[134]

Crooks *et al.* have recently pioneered the use of electrocatalytic amplification (ECA) for the detection of miRNA.[135–138] In their recent study they designed a system in which the target miRNA hybridises to its complementary ssDNA immobilised on a platinum nanoparticle surface (Fig. 10).[72] Once in its duplex, it is then susceptible to degradation by duplex specific nuclease (DSN) enzyme, thus exposing the platinum nanoparticle surface. Additionally, the miRNA is left intact, and may further interact with other immobilised ssDNA molecules. Individual collisions of the exposed catalytic platinum nanoparticles with the non-catalytic electrode surface result in observed current transients for the oxidation of hydrazine (N_2H_4). Using this technique, miRNAs overexpressed in tumor cells could be detected with a limit of detection (LOD) of 100 pM.

One limitation of DNA switches for sensing applications is that the conventional signalling mechanisms of molecular beacons typically limits the detection limit to the picomolar
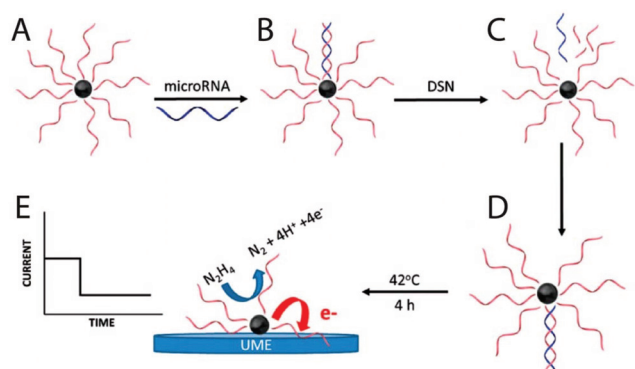
**Fig. 10** miRNA detection using electrocatalytic amplification (ECA). (A) The surface of a platinum nanoparticle is modified with a monolayer of ssDNA, which prevents current transients during nanoparticle-electrode collisions. (B) Target miRNA hybridises with the complementary ssDNA. (C) DSN enzyme cuts the DNA : RNA hybrid, (D) and also releases the miRNA that can further hybridise with another immobilised ssDNA. (E) When enough ssDNA is removed from the platinum nanoparticle, current transients are observed when it collides with the electrode surface. Adapted with permission from ref. 72. Copyright 2017 American Chemical Society.

Fig. 11 Tetrahedral DNA electrochemical biosensors with amplification strategies for nucleic acid detection. (A) Binding of the target miRNA opens the molecular beacon, which exposes a segment complementary to the silver nanoparticle-labelled signal probe. A Klenow fragment then polymerises the signal probe, which displaces the target miRNA that is recycled for continuation of the process. (B) Binding of the target to the probe occurs, followed by amplification of the hybridisation signal *via* biotin-modified H1 ad H2. Lastly, avidin-modified HRP is attached to the HCR products to produce an electrocatalytic signal. Panel A is adapted with permission from ref. 139. Copyright 2015 American Chemical Society. Panel B is adapted with permission from ref. 86. Copyright 2014 American Chemical Society.

concentration range. To circumvent this limitation *via* amplification of the signal, Miao *et al.* have developed an electrochemical biosensor for miRNA detection that uses a thiol-immobilised tetrahedral DNA on a gold electrode (Fig. 11A).[139] A stem-loop structure, complementary to the target miRNA, is inserted at the top of the tetrahedron. Upon binding of the target, a portion of the opened stem-loop sequence is exposed, and will bind a signal probe that is labelled with a 4 nm silver nanoparticle. In the presence of the silver nanoparticle-labelled signal probe, an electrochemical signal can be obtained. Furthermore, a Klenow fragment will initiate polymerisation of the signal probe, thus displacing the target miRNA, which can in turn be recycled for further detection *via* other molecular beacons on the surface. This system has a LOD of 0.4 fM, and can discriminate the target from mismatched miRNAs. Furthermore, its clinical potential was demonstrated by detection of miRNA in serum samples from breast cancer patients.[139] Elsewhere, Ge *et al.* have developed a system combining a tetrahedral DNA scaffold switch with a HCR to enable the ultrasensitive detection of DNA and miRNA, with LODs in the attomolar regime, thus demonstrating the great potential of this amplification strategy (Fig. 11B).[86] In their system, the target DNA or miRNA hybridises onto a surface-immobilised probe, followed by alternating attachment of two biotin-modified hairpins that hybridise to continue the DNA duplex, which stops upon exhaustion of the hairpins. Avidin-conjugated horseradish peroxidase (avidin-HRP) attachment to the biotinylated probe *via* the hybridised hairpins thus allows for electrochemical measurement *via* the catalytic reduction of H_2O_2.[86] Other recent amplification strategies for electrochemical detection of DNA and miRNA have also employed DNAzymes.[140]

Detection of specific DNA sequences is useful for medicine applications, as well as in biotechnology and forensics. However, one major challenge is the discrimination of target DNA from DNA with single nucleotide mutations (SNMs). Hu *et al.* recently reported a strategy consisting of a target-specific fluorophore/quencher-labelled molecular beacon and a series of rationally-designed unlabelled hairpin sequestering agents (SEQs) that sequester their corresponding single-base mismatched sequences (MMs) (Fig. 12).[141] The molecular beacon binds its perfectly matched target sequence (PM), thus opening the molecular beacon and giving a rise in fluorescent signal. On the other hand, in the presence of MMs only, the molecular beacon remains in the closed state since the MMs are captured by the SEQs. Finally, in the presence of both, the PM and MMs are captured by the molecular beacon and the SEQs, respectively. This assay shows a remarkable discrimination ability for a variety of sequences with SNMs. It was applied in a clinical setting in conjunction with PCR for detection of mutated KRAS genes, which are associated with various types of cancer.[141] Inspired by natural structure-switching mechanisms, the specificity for target DNA can also be
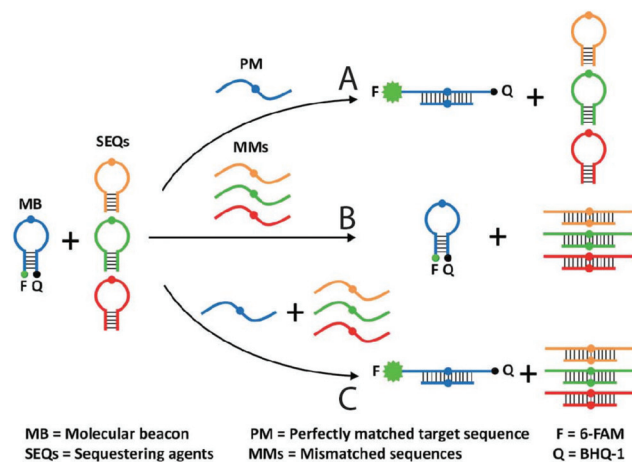
Fig. 12 Operation principle of the sequestration-assisted MB strategy for MM discrimination. In (A) the PM is captured by the MB, and in (B) the MMs are captured by the SEQs. In (C) the PM is captured by the MB, and the MMs are sequestered by the SEQs. Adapted from ref. 141. Published in 2017 by The Royal Society of Chemistry.

boosted by a 10-fold increase *via* a triplex clamp-switch binding of the target. In this design, the target is bound by both Watson–Crick and Hoogsteen interactions.[142]
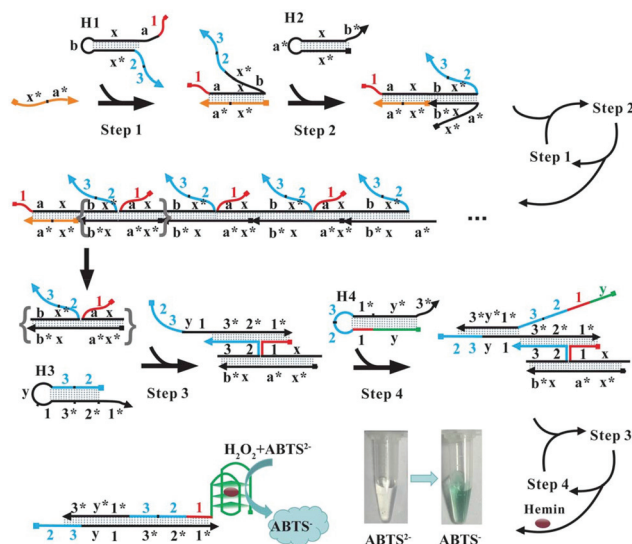
As an alternative to typical organic fluorophore/quencher pair labels, Engelen *et al.* achieved DNA detection in the low picomolar regime using a system based on bioluminescence resonance energy transfer (BRET) between a bioluminescent luciferase enzyme (NanoLuc) and Cy3 acceptor dye (Fig. 13).[143] NanoLuc is conjugated at the 5′-end of a handle sequence, and the Cy3 at the 3′-end of the anti-handle sequence in the shape of a molecular beacon. Bioluminescence is quenched *via* BRET due to the close spatial proximity of the NanoLuc and Cy3, but treatment with the target DNA opens the hairpin to give a signal. This approach allows for use of the same NanoLuc and handle DNA with different Cy3-labelled probe DNAs, thus achieving programmability for different targets. Linear signal was observed over the 0 to 500 pM range, with a LOD of 6 pM. Additionally, a 22 nucleotide deoxyribose analog of a miRNA associated with cancer was detected in serum.[143] From

another approach, sequence-dependent fluorescent DNA-stabilised silver nanoclusters were used by Ge *et al.* to achieve ratiometric detection of a target sequence down to 8.5 pM.[144] Appealingly, these DNA/Ag nanocluster sensors do not require expensive fluorophore/quencher pair dual-labelling (see also recent a review by Yuan *et al.*[76]).

Colourimetric biosensors are very attractive tools due to their simplicity and cost-efficiency. Very recently, Bai *et al.* introduced a colourimetric amplification-based DNA sensor to detect and quantify nucleic acids or proteins without the need of any DNA modifications or enzymes.[145] This strategy is based on previous advances in DNA nanotechnology[146] that combine signal amplification by catalysed hairpin assembly (CHA)[147] in response to an HCR[148] product with single-stranded extensions forming an associative toehold.[58] The operation principle of this biosensor is illustrated in Fig. 14. First, the nucleic acid analyte hybridises with hairpin H1, opening it and initiating a HCR with hairpin H2 (steps 1 and 2). The multiple single stranded extensions co-localised in the HCR product then act together as toeholds and branch migration domains to catalyse multiple rounds of assembly between hairpins H3 and H4 (steps 3 and 4). In this H3–H4 duplex, the G-quadruplex forming sequence is exposed and folded, allowing the oxidation of colourless $ABTS^{2-}$ to green $ABTS^-$ in the presence of H_2O_2 and hemin. With a high specificity against proximal mismatches, a detection limit of 0.14 pM, and quantitative linearity between 1 pM and 75 nM of target DNA, this colourimetric approach may find applications in mutation analysis, diagnostic analysis and forensic testing. Using the proximity-triggered hybridisation mechanism[54] to bring together the toehold and branch migration domains of the input DNA in the presence

Fig. 13 Design of the intermolecularly assembled BRET-beacon. A handle-strand is conjugated to NanoLuc, which then hybridises with an anti-handle strand appended to the target-binding stem-loop. The acceptor fluorophore (Cy3) is used to measure BRET efficiency. Binding of the target oligonucleotide by the stem-loop seperates the NanoLuc and Cy3, thus decreasing BRET efficiency. Reprinted from ref. 143. Published in 2017 by The Royal Society of Chemistry.

Fig. 14 Operation principle of the amplification-based colourimetric biosensor employing catalysed hairpin assembly (CHA, steps 3 and 4) triggered by HCR assembly of associative toeholds (steps 1 and 2) for sensitive detection of nucleic acid analytes (orange strand). Reprinted with permission from ref. 145. Copyright 2017 Elsevier B.V.

of an aptamer target, this strategy can also be employed to detect non-nucleic acid analytes.

3.2.3. Heavy metal ions. An unwaveringly popular field of analytical chemistry involves the detection of metal ions.[16,149,150] Specific DNA sequences have been shown to specifically bind metal ions such as Hg^{2+} and Ag^+. For example, a thymine–thymine mismatch within a duplex helix forms a stable $T–Hg^{2+}–T$ base pair,[15] while a cytosine–cytosine mismatch forms a stable $C–Ag^+–C$ base pair.[17] Using these attributes, Porchetta *et al.* developed allosterically-tunable fluorescent DNA switches for the detection of Hg^{2+} and Ag^+ (Fig. 15) which, through addition of specific DNA strands, can display different dynamic ranges.[100] By taking advantage of the $T–Hg^{2+}–T$ base pair, Chen *et al.* have developed a disposable strip biosensor for the visual detection of Hg^{2+}.[151] Their design employs an amplification strategy that uses an enzyme-based toehold-mediated strand displacement reaction in combination with gold nanoparticles (Fig. 16). This visual colourimetric assay allows for simple and rapid, on-the-spot analysis of samples outside of the laboratory down to 1 pM Hg^{2+}, which the authors note is well below the 10 nM maximum concentration of Hg^{2+} allowed in drinking water in the USA. The assay displayed high specificity and selectivity, and its low cost ($1.50 for a single strip analysis) renders it attractive for commercial use beyond academia. Other DNA-switch based sensing strategies have also been developed for the detection of the mining byproduct thallium (Tl^+ oxidated state)[13] as well as for Hg^{2+},[152] Ag^+,[153] Ag^+ and Pb^{2+},[154] Hg^{2+} and Pb^{2+},[155] Zn^{2+},[156] S^{2-},[157] and UO_2^{2+} ions.[158] Cr^{3+} ions have also recently been used with molecular beacons to replace the organic quencher.[159]

3.2.4. Small molecules. DNA aptamers that have been selected to bind any desired targets with high affinity and specificity[22–26] can be readily adapted for a variety of
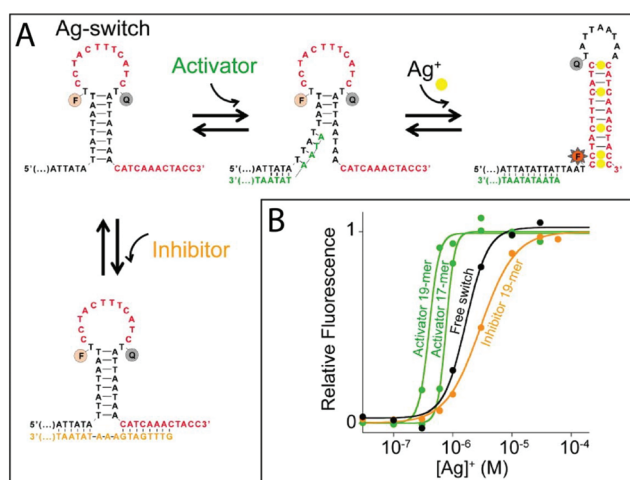
Fig. 15 A programmable Ag^+ fluorescent sensor. (A) Allosteric activators and inhibitors are employed to destabilise and stabilise, respectively, the nonbinding conformation of the DNA switch, which (B) tunes the dynamic range to lower or higher Ag^+ concentrations. Adapted with permission from ref. 100. Copyright 2013 American Chemical Society.
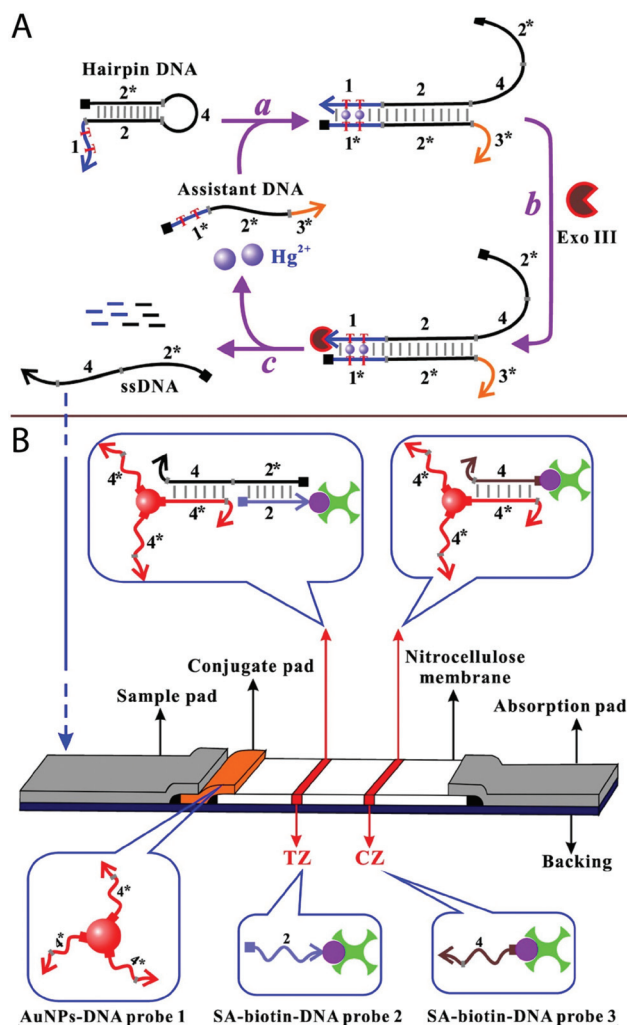
Fig. 16 Disposable strip biosensor for visual detection of Hg^{2+} ions. The Assistant DNA hybridises to the Hairpin DNA, which is complementary except for the T–T mismatches used to bind Hg^{2+}. The open hairpin is then degraded by Exo III, thus releasing the Hg^{2+} and the Assistant DNA. The ssDNA generated from the enzymatic reaction hybridises with a Au nanoparticle-conjugated Probe DNA that migrates along the strip, ultimately giving rise to a red band (TZ). This can only occur in the presence of Hg^{2+}, since the Exo III-assisted reaction is specific for the open hairpin. A control band (CZ) forms regardless of the target's presence. Adapted with permission from ref. 151. Copyright 2014 American Chemical Society.

biosensors.[51,117,126–128,160–162] As a case study, we discuss several recent developments involving the DNA switches leveraging the aptamer for cocaine (see also allosteric tuning of the cocaine aptamer discussed in section 2.4.1).[49,99] Electrochemical aptamer-based (E-AB) sensors typically involve an electrode-bound aptamer that contains a redox-reporter that can detect, upon binding of its target, conformational modifications *via* a change in measured current.[61,111,123,163] However, this strategy typically suffers from significant baseline drift when employed directly in whole blood, likely because of non-specific adsorption of red blood cells onto the electrode. To get around this problem, Li *et al.* recently

designed a dual-reporter strategy wherein the E-AB sensor contains two redox reporters on the aptamer (Fig. 17A).[163] Crucially, both redox reporters exchange electrons at potentials that do not overlap. Furthermore, their stability and physical properties allow them to respond similarly to signal drift. The sensing reporter, methylene blue, is placed on the end of the aptamer away from the surface. Target binding-induced conformational changes bring it into closer proximity to the surface, resulting in electron transfer and detection of the target molecule. The reference reporter, anthraquinone, remains close to the electrode surface in either conformation, thereby keeping its signal constant. In a 15-hour flowing whole blood experiment, the signal drifts for both reporters were about 25–30%. However, after a drift correction was taken into consideration, corrected signal drift was only 2%. This sensing strategy was found to be generalisable for many aptamers such as the cocaine-, aminoglycoside- and doxorubicin-binding aptamers.[163]

Sensing of small molecules directly in the bloodstream would provide a vital tool for personalised medicine through monitoring of patient health and response to therapeutics. However, aptamer sensing devices typically suffer from non-specific signal drift when immersed in whole blood. Accordingly, Ferguson *et al.* developed a real-time biosensor for continuous monitoring of aptamer-specific targets in living subjects' blood that self-corrects for signal drift.[164] The system, called a microfluidic electrochemical detector for *in vivo* continuous monitoring (MEDIC) was adapted for the continuous monitoring of the cancer drug doxorubicin (DOX) in sedated live rats. The system works for several hours with sub-minute temporal resolution, self-corrects for signal drift, uses a disposable chip format, and provides pharmacokinetic para-

meters for individual animals in real-time.[164] While described as "*in vivo*", this approach was nonetheless an "*ex vivo*" method because blood flowing through the device could not be re-injected into the subject since it was slightly diluted with buffer. More recently, Li *et al.* solved this problem by developing a cell membrane-mimicking phosphatidylcholine-based sensor that does not require membranes nor algorithms to prevent signal drift for *in vivo* monitoring of DOX in rats.[165]

Yu *et al.* have recently developed a new approach for fluorescence-based DNA aptamer detection of cocaine (Fig. 17B).[166] The background of this DNA switch can be reduced by splitting the aptamer into two fragments that cannot assemble in the absence of the target, however this comes with the price of lower affinity for the target. By including two cocaine-binding domains in the cooperative binding split aptamer (CBSA), cooperative binding is achieved wherein the first cocaine-binding event stabilises the aptamer, thus leading to subsequent binding at the second binding site. This approach was found to be superior to the single-binding domain design from which it was derived. The cooperative binding mechanism of the switch could be confirmed by disrupting either of the binding domains through a single-nucleotide mutation, thus leaving only one available for the binding of cocaine. This assay is sensitive for detection of cocaine in saliva samples with a LOD of 50 nM, which they noted surpasses the requirements of the European Union. In addition to being highly specific, the per test cost of this assay is reported to be only $1.28.[166]

Another class of small molecules of concern for health considerations are pesticides found in water and food for human consumption. To address this challenge, Wang *et al.* recently developed a DNA-based electrochemical immobilisation-free assay that employs the high molecular recognition properties of enzymes for the detection of organophosphorus pesticides, such as diazinon (Fig. 18A).[167] In this system, a DNA strand labelled with methylene blue acts as an electrochemical reporter (shown as HP for helper probe). This HP strand can form a hairpin structure *via* T–Hg^{2+}–T base pairing. Diazinon can inhibit acetylcholinesterase (AChE) present in the system, which in the absence of the pesticide catalyses the hydrolysis of acetylthiocholine chloride (ATCh) to thiocholine (TCh) in order to sequester Hg^{2+} ions also present. HP can then form a random coil that is degraded by Exo I, ultimately resulting in the release of a methylene blue-labelled mononucleotide, which is then detected *via* SWV. Therefore, the signal decreases with increasing concentrations of diazinon. While this assay was shown to be sensitive for other organophosphorus pesticides with a reported LOD for diazinon of 0.25 μg L^{-1} (0.82 nM), it remained insensitive to other kinds of pesticides and inorganic ions. The authors further demonstrated the potential of the assay for food safety applications by using diazinon spiked in lake water and apples.[167] Using similar principles, a fluorescence-based system was also developed for the carbamate pesticide aldicarb in fresh ginger and lake water,[168] as well as an RCA-based electroanalytical system for pesticides in peach and carrot samples; thus demonstrating
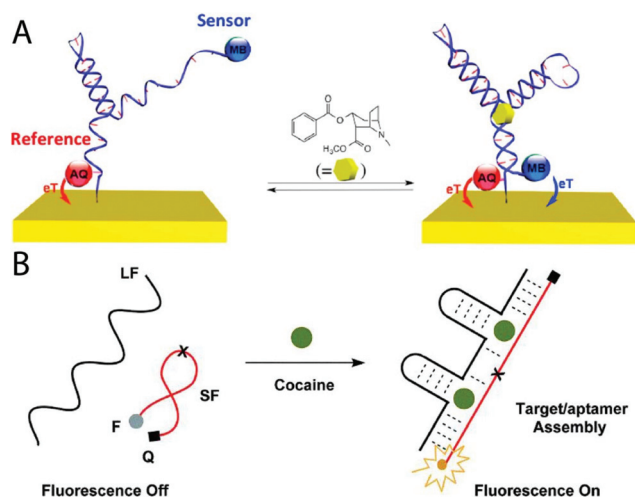
Fig. 17 DNA switch for cocaine detection. (A) Electrochemical aptamer-based sensor with dual-reporter drift correction for detection in whole blood. (B) The design of the cooperative binding split aptamer (CBSA) assay. Panel A adapted with permission from ref. 163. Copyright 2016 American Chemical Society. Panel B adapted from ref. 166. Published in 2017 by The Royal Society of Chemistry.
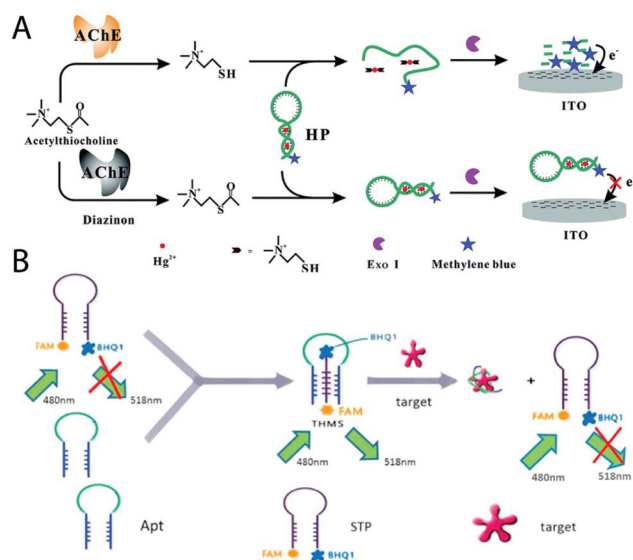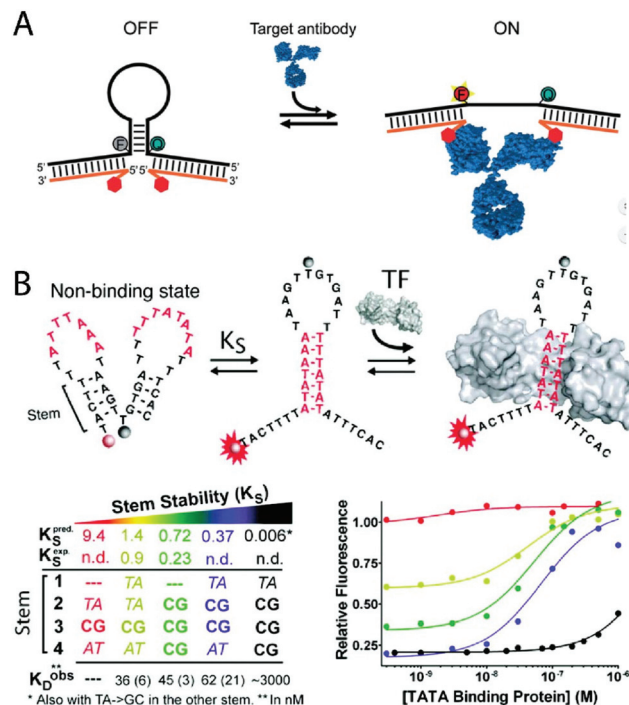
Fig. 18 Methods for detection of pesticides in food samples. (A) Homogeneous electroanalytical detection of organophosphorous and carbamate pesticides based on a acetylcholinesterase inhibition and Hg^{2+}-mediated DNA switching, combined with Exo I nicking enzyme. (B) Aptamer-based triple-helix molecular switch (THMS) method of detection. Panel A adapted with permission from ref. 167. Copyright 2016 The Royal Society of Chemistry. Panel B adapted with permission from ref. 170. Copyright 2016 Elsevier B.V.

Fig. 19 Universal DNA switch-based switches for the detection of antibodies (A) and transcription factors (B). (A) A universal antibody-activated switch that enables the fluorescent detection of any antibody by simply replacing the small (<20 kDa) recognition element (red hexagon) in the DNA–epitope conjugate (orange strand). (B) A universal transcription factor-activated switch that enables the fluorescent detection of any transcription factor by employing the specific double-strand DNA sequence recognised by the transcription factor. Panel A adapted with permission from ref. 173. Copyright 2015 Wiley-VCH. Panel B adapted with permission from ref. 175. Copyright 2011 American Chemical Society.

real life applications[169] Elsewhere, Liu *et al.* developed a fluorescence-based method for detection of the broad spectrum insecticide acetamiprid (Fig. 18B). This method uses an aptamer-based triple-helix molecular switch (THMS), which releases the signal transduction probe (STP) after the aptamer binds the target. High selectivity was observed in the presence of structurally similar compounds, as well as ions and chemicals typically found in vegetable samples. The LOD of this method was 9 nM, and in Chinese cabbage the LOD was 3.5 μg kg^{-1}; below the maximum acceptable limit.[170]

3.2.5. Proteins. Proteins, like small molecules, can also be efficiently detected using aptamer-based sensors.[23,26,39,117–125,171,172] Companies like Somalogic, for example, have started to commercialise hundreds of DNA aptamers (or SOMAmers)[29,30] that specifically recognise human proteins with affinities and specificities similar to antibodies. However, the aptamer selection process does not represent the most efficient strategy to generate recognition elements for many families of proteins. For instance, antibodies typically recognise small epitope moieties from peptides, sugars or other molecules. Transcription factors, another example, recognise specific double-stranded DNA sequences. Why not then build DNA switches using these already available recognition elements?

With this idea in mind, Ranallo *et al.* have developed a universal DNA switch for the detection of antibodies (or any bivalent protein) (Fig. 19A).[173] This stem-loop switch contains a fluorophore/quencher pair and is easily labelled with a specific epitope known to recognise its antibody through hybridisation with a DNA–epitope conjugate. Upon binding to its target antibody, the switch opens up, thus separating the fluorophore/quencher pair. In this work, switch thermodynamic optimisation was performed in order to lower the background fluorescence of the switch without overly stabilising the stem and having two antibodies binding one closed stem. Target detection of five bivalent proteins in 100% serum was demonstrated, including detection of an HIV antibody. This switch has also been easily adapted in an electrochemical format.[174]

Another programmable DNA switch architecture has been developed by Vallée-Bélisle *et al.* for the detection of transcription factors, an important class of proteins that control crucial biological mechanisms such as cell proliferation and apoptosis (10% of the ~25000 human genes encode DNA-binding proteins, the majority of which function as transcription factors) (Fig. 19B). This switch shifts from a non-fluorescent double stem-loop non-binding state to a fluorescent single stem binding conformation that displays the double-stranded DNA sequence recognised by a specific transcription factor. As with many DNA switches, fine tuning of the switching equilibrium

was found to be a key determinant of switch performance (optimal detection limits were obtained with K_S between 1 and 0.1). This switch was adapted for the detection of three different transcription factors, and enables the measurement of transcription factor concentration directly in nuclear extract.[175]

Wei *et al.* have developed a system based on Mg^{2+}-dependent DNAzymes (MNAzymes) with a proximity ligation assay (PLA) for protein detection. In this system, probe A and probe B each possess an aptamer sequence recognizing the protein target (platelet derived growth factor BB; PDGF-BB), a polyT spacer, a short stem sequence, and part of the MNAzyme. A DNA linker containing the MNAzyme's substrate sequence is designed to connect two DNA-modified gold nanoparticles. Without the PDGF-BB, the stems cannot hybridise to each other due to their low T_m, and the MNAzyme cannot form. The linker strand can then hybridise with the gold nanoparticles' strands, resulting in their change of colour from red to purple. Conversely, binding of the protein results in the gold nanoparticle colour remaining red. In addition to a low LOD (1 pg mL^{-1}) and high specificity in the presence of other proteins, this "mix-and-detect" colourimetric strategy worked well in serum.[177] For further discussion of sensors for proteins based on DNA assembly and affinity binding, the reader is directed to a review article by Zhang *et al.*[54]

Multiplexed detection strategies ought to allow for simultaneous detection of multiple markers of the same disease, or alternatively, more than one disease during a single analysis. To achieve this feature, Xu *et al.* developed a system using SERS, and demonstrated the simultaneous detection of three protein markers (prostate specific antigen (PSA), thrombin, and mucin-1) directly in serum at physiologically-relevant concentrations (Fig. 20). In their single-target design, four silver nanoparticles are coated with a Raman reporter 4-aminothiophenol (4-ATP), and connected by a "DNA frame" consisting of the PSA aptamer to produce a Ag-pyramid. Binding of PSA by the PSA aptamer decreases the gap between the adjacent nanoparticles through a structure-switching mechanism, thereby enhancing the Raman signal of the 4-ATP (Fig. 20A). Furthermore, by covering three nanoparticles with different Raman reporter molecules that have distinct vibrational signals (4-ATP, 4-nitrothiophenol (NTP), or 4-methoxybenzyl mercaptan (MATT)), and by forming the pyramid *via* differing aptamers, the system can also be used for multiplexed sensing of PSA, thrombin, and mucin-1 (Fig. 20B). In a sample containing all three proteins, the LOD values for PSA, thrombin and mucin-1 were 0.96 aM, 85 aM and 9.2 aM, respectively, with the differences attributed to the relative dissociation constants (K_d) of the proteins.[176] Elsewhere, Su *et al.* developed a dual-target electrochemical aptasensor for thrombin and adenosine triphosphate (ATP), wherein their respective aptamers with separate redox tags are immobilised on a gold nanoparticles–MoS$_2$ nanocomposite. To provide fewer misreadings and high sensitivity, this detection strategy uses signal-off and signal-on sensing mechanisms for thrombin and ATP, respectively, and for both
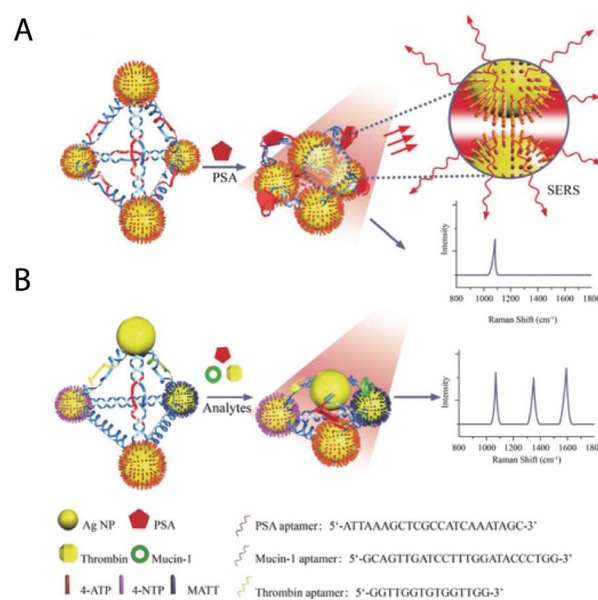
Fig. 20 SERS analysis of protein biomarkers. (A) SERS assay for PSA, with 4-ATP-modified silver nanoparticles and the frame connected by PSA aptamers. (B) SERS multiplexed assay for PSA, thrombin and mucin-1 with their silver nanoparticles modified with 4-ATP, NTP and MATT, respectively, and the three protein aptamers connecting three sides of the DNA frame. Adapted with permission from ref. 176. Copyright 2015 Wiley-VCH.

molecules limits of detection in the nanomolar regime were achieved.[178]

4. Switches for probing biochemical processes

Owing to their nanometer size and biochemical nature, DNA switches represent ideal tools to interact with biomolecules and to monitor dynamic biological processes *in situ*. Their ability to fluorescently signal the presence and localisation of selected molecules or processes, combined with imaging techniques such as confocal microscopy, allows us to monitor molecular activity in living cells. Since the fluorescent signal is specifically and reversibly triggered by the target, switches can probe living systems in real-time with low background signal, circumventing the need for cross-linking cells and washing excess unbound probes, which is commonly encountered with *in situ* fluorescence hybridisation (FISH) or immunofluorescence studies. Fluorescent DNA probes also expand the repertoire of flow cytometry analysis by distinguishing live cells based on their gene expression profiles rather than being limited to cell surface markers. Moreover, they allow for non-destructive analysis, thus enabling recovery of living cells after sorting, and bypassing the need to run parallel experiments to gather information over time.[179]

Nucleic acid sensors are typically delivered into living cells through electroporation techniquess, by induction of pores in

the membrane using bacterial toxins, by conjugation to cell-penetrating peptides, through the use of aptamers, micelle-forming lipids or gold nanoparticles, and also by means of microinjection.[180–182] Conjugation to nanoparticles can provide nuclease resistance and high stability against degradation in biological environments,[182,183] supporting long-term intracellular monitoring over more than 2 weeks.[184–186] DNA/RNA switches can also be made more resistant to nuclease degradation by employing various chemical modifications, such as modification of the phosphorothioate backbone, the incorporation of a methylated nucleobase or its oxidised variant, the use of fluorine-modified ribose, phosphorylation at the 3′ terminus, or finally by the incorporation of inverted dT or dideoxythymine (ddT). In this section, we cover the most recent advances in the use of nucleic acid switches to further our understanding of living systems. As this is not an exhaustive review of the subject, readers are directed to other complementary reviews on this topic.[1,116,182,187–193]

4.1. Probing cells

4.1.1. Single cell analysis. Most of our knowledge of gene regulation is derived from averaged measurements on cell populations.[194,195] However, even with cells of an identical genetic background, it is becoming increasingly evident that cell-to-cell variability in gene expression drives certain biological phenomena; the causes of which would otherwise be masked by ensemble measurements.[195] For example, antibiotic resistance,[196] tumorigenesis[197] and stem cell differentiation[198] all involve outlier cells driving the overall process. Moreover, certain genetic mutations associated with diseases may not result in altered mean expression levels, but affect variability of expression among cells.[199] Therefore, measuring gene expression at the single-cell level is expected to reveal the dynamics of rare but important regulation events involved in disease or differentiation. In this context, DNA switches offer a ready means to quantify RNA in real-time and in single living cells using fluorescence microscopy or flow cytometry.

Molecular beacons are useful tools to specifically mark subsets of cells based on their gene expression levels. Ban *et al.* recently demonstrated isolation of a specialised subtype of cardiac cells by flow cytometry based on the detection of a precise mRNA using molecular beacons.[200] This approach overcomes the challenges of isolating cell-types lacking specific surface markers necessary for antibody-based cell sorting. Molecular beacons can also be used to simultaneously monitor multiple mRNA or miRNA in real-time inside single differentiating stem cells, and has been applied to neuronal, osteogenic, adipogenic and myogenic cell types.[179,185,200–202] Down the line, the ability to non-invasively report early stages of differentiation could be used as a tool for high throughput screening of efficient differentiation conditions. Moreover, isolating subpopulations of specialised cells without resorting to destructive methods (*e.g.* FISH) enables downstream characterisation of these cell types. Molecular beacons have also been used to quantitatively and simultaneously assess temporal changes in the expression of genes critical for drug response

in subpopulations of living cancer cells,[203,204] and multiplexed gene expression platforms are envisioned to analyse and understand drug resistance.[191]

Genetically-encoded artificial RNA switches are paving the way for real-time imaging of small molecules and proteins in single living cells without the need to deliver the switches. By performing SELEX to identify RNA aptamers that bind to conditionally fluorescent dyes, Paige *et al.* have identified a green aptamer–dye complex, termed Spinach, which contains three stem-loops encircling a central loop enclosing the dye (Fig. 21).[205] Mutagenesis revealed that formation of one of these stems was essential for the aptamer structure and fluorescence of the complex. By destabilising this stem and fusing it to a second structure-switching aptamer, the authors created a binding-induced fluorescent system where folding of the second aptamer in the presence of ligand closes the stem and activates fluorescence (Fig. 21).[206] Virtually any kind of molecule could be detected by fusing different aptamers to Spinach. For example, natural riboswitches can be fused with Spinach to produce metabolite sensors that exploit the natural diversity of ligand binding riboswitches. Spinach riboswitches have enabled real-time single-cell measurement of adenosine, guanine, SAM and TPP metabolite concentrations[208] as well as proteins.[209] Cell-to-cell variability in bacterial metabolism was readily detected, and has been linked to antibiotic resistance.[210] Spinach riboswitches are also able to specifically recognise known agonists and antagonists of its natural riboswitch counterpart. This property could be useful for identifying new agonists or antagonists by simple *in vitro* fluorescence assays, instead of the usual GFP or other reporter gene assays.

4.1.2. Probing cellular subcompartments. DNA switches can also be adapted to monitor analytes in subcellular organelles by conjugating them to various targeting moieties that are recognised by cells and internalised in specific compartments (reviewed in more detail in ref. 189). The use of DNA switches for imaging live cell compartments was demonstrated by Modi *et al.* who engineered a DNA tweezer with both arms forming a pH-dependent i-motif (Fig. 22).[211] The mul-
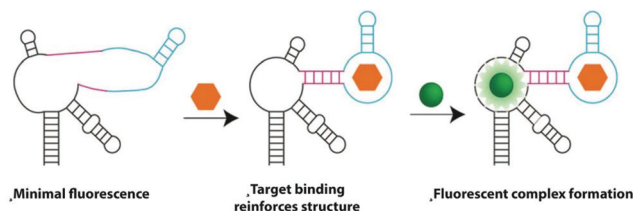
Fig. 21 Modular strategy for engineering the genetically encoded RNA sensor Spinach. Spinach is an RNA aptamer (black) that binds a small molecule dye called DFHBI (green) which only emits fluorescence when bound. One stem-loop (magenta) is essential for the structure and fluorescence of the complex. To generate a sensor, this stem-loop is fused to a recognition module (blue), a second aptamer or riboswitch. Upon target binding (orange), folding of the recognition module induces folding of the stem-loop. Spinach is then able to bind DFHBI and activate fluorescence. Adapted with permission from ref. 207. Copyright 2014 Macmillan Publishers Ltd.
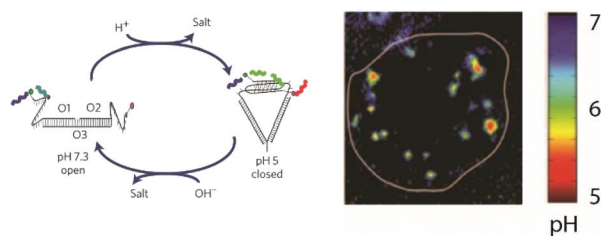
Fig. 22 Working principle of the pH sensing I-switch. (A) Formation of the i-motif at low pH closes the tweezer and produces a high FRET signal (red). At higher pH, disruption of the i-motif leads to dissociation of the two arms, opening the switch and producing a low fret signal (blue). (B) Pseudocolour map of FRET donor/acceptor intensities inside a haematocyte 2 hours after being pulsed with I-switch. Adapted with permission from ref. 211. Copyright 2009 Macmillan Publishers Ltd.

tiple negative charges of the DNA phosphate backbone allow it to be endocytosed through the anionic ligand binding receptor (ALBR). The I-switches were found to be localised inside defined punctate structures corresponding to endosomes, and their gradual acidification over time could be quantified. Through protein conjugation, it was also possible to target the switch to different endocytic pathways, and image the vesicle networks and lumenal pH. Using two DNA switches targeting different endocytic pathways, they further demonstrated simultaneous spatiotemporal pH mapping of two endocytic pathways in the same living cell.[212] Segregation of the two endocytic pathways at later times could be visualised, as well as defects in endosome morphology and dynamics induced by chemical inhibition. Approaches for imaging endosomal pathways and their content are likely to bring deeper insight for many adverse physiological conditions, for example in the case of Alzheimer's disease or atherosclerosis, which involve defects in endocytosis.[214]

## 4.2. Imaging single molecules inside cells

DNA switches can also help monitor cellular mRNA trafficking. For example, Alami *et al.* used nuclease-resistant molecular beacons to image real-time *in vivo* trafficking of a specific mRNA found in messenger ribonucleoprotein particles (mRNP) granules over a period of 2 weeks.[184] This approach revealed axonal transport defects of mRNA in cells from amyotrophic lateral sclerosis (ALS) patients, and allowed characterisation of the underlying mutations. However, imaging single molecules that do not form clusters can be challenging due to low fluorescence signals. While single RNA molecules can be visualised by genetically inserting tandem repeats in their sequence and targeting these repeats with molecular beacons to generate sufficiently high signal per molecule,[215,216] such inserts may also affect localisation, trafficking, degradation and concentration, therefore limiting applications of this method.[217,218] Since imaging of endogenous RNA is generally preferable, Deng *et al.* have introduced a strategy termed TIRCA (toehold-initiated rolling circle amplification) that enables amplification of the fluorescence signal for imaging a single endogenous RNA molecule (Fig. 23).[213] Initially, the
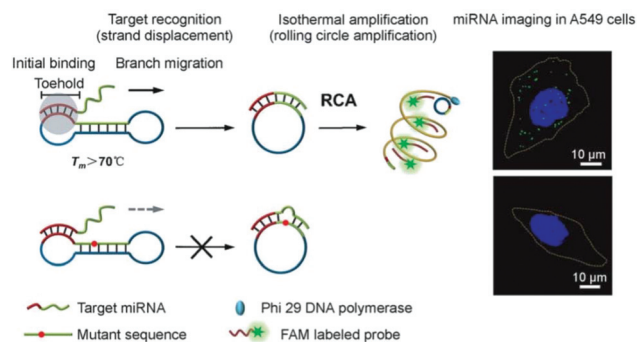
Fig. 23 Schematic representation of TIRCA for visualising individual endogenous RNA molecules *in situ*. Top: Binding of the toehold domain to the target RNA opens the circular probe through strand displacement and initiates rolling circle amplification (RCA). Hybridisation of the amplification product with multiple fluorescent probes leads to a bright spot for each RNA molecule recognised. Bottom: Mismatched RNA fails to branch migrate through the probe and does not trigger amplification. Reprinted with permission from ref. 213. Copyright 2014 Wiley-VCH.

self-complementary DNA circle forms an intramolecular duplex; a closed state that cannot serve as the template for phi 29 DNA polymerase. Binding of the target miRNA to the toehold domain initiates strand displacement of the duplex, opening the circle and activating rolling circle amplification (RCA). For each target miRNA, hybridisation of the newly synthesised DNA with many fluorescent DNA probes leads to a bright spot that can be visualised by microscopy.

Visualisation of single proteins *in situ* has also been made possible by the signal amplification capacity of DNA switch systems. Previous approaches for imaging single proteins typically involved genetic fusions that recruit several fluorescent proteins[221] but these genetic manipulations could perturb the localisation or function of the target. Based on the proximity ligation assay,[222] Koos *et al.* recently developed a proximity-based hybridisation chain reaction (proxHCR) where the adjacent binding of two different antibodies conjugated to complementary DNA hairpins triggers a fluorescent HCR (Fig. 24).[219] The HCR is initiated by a single stranded activator that invades the first proximity hairpin, exposing a sequence
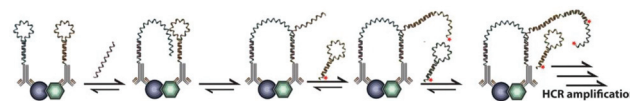
Fig. 24 ProxHCR strategy for single molecule imaging of endogenous proteins. Two different primary antibodies bind interacting proteins, bringing the two hairpins into close proximity. The activator strand opens the first hairpin, which subsequently invades and opens the second hairpin. The exposed sequence of the second hairpin acts as the initiator for the hybridisation chain reaction (HCR) by binding and opening a fluorescently-labeled hairpin, which in turn binds and opens a second fluorescent hairpin. The second hairpin is also able to open other fluorescent hairpins of the first kind, and the HCR reaction continues until there is no more fluorescent hairpin left to hybridise.[219] Figure adapted with permission from ref. 220.

that invades the second proximity hairpin. Invasion of the second proximity hairpin, in turn, exposes a sequence that triggers a hybridisation chain reaction (HCR) opening multiple stem-loop fluorescent probes,[148] thereby providing sufficient signal to detect single molecules inside cells. Using a similar strategy, one can also monitor protein–protein interactions with two antibodies or aptamers each targeting a different protein.

4.3. Probing membrane-associated processes

The cell membrane hosts important cell–cell communication and environment sensing functions. These functions in turn regulate critical cellular responses like proliferation, differentiation, migration, metabolism and immunity, among others. The cell membrane also represents a potential interface by which we can manipulate and program cellular activities. While a fundamental understanding of membrane biology would greatly improve our ability to interact with cells, monitoring dynamic membrane-associated molecules with high spatial and temporal resolution remains a challenge. Current methods to assess the composition of membranes, such as western blotting, mass spectrometry and immunofluorescence microscopy, either require considerable sample preparation or do not provide spatial and temporal resolution.

A potential solution to the challenges of investigating interactions on cell membranes is presented by You *et al.* who used toehold strand displacement to report encounters between specific molecules on cell membranes.[223] Using pairs of fluorescent and quencher toehold switches covalently linked to different lipid anchors, they monitored transient encounter rates between pairs of diffusing lipids in live cell membranes. The experiment begins with the displacement of a protecting strand from the anchored quencher strand, revealing the complementary sequence to the fluorescent strand's toehold. Following this, encounters between the two lipids initiates strand displacement of the unlabeled anchor strand to yield a quenched duplex (Fig. 25). Lipid encounter rates were shown to be dependent on the nature of the interacting lipids, with more frequent collisions between similar lipids or lipids that partition the same domains in model membranes, thus supporting the lipid raft theory. The increased encounter rate of lipids confined in membrane domains compared to a freely-diffusing model allowed estimation of the percentage of cell surface area covered by lipid domains. Finally, the authors demonstrated that this method can also be applied to monitor rapid encounters between membrane proteins by tethering them to toehold probes with aptamer sequences. Because the encounter rates were found to be sensitive to the orientation of the DNA strands, as it depends on which species initially carries the fluorescent or quencher toehold, this strategy may allow determination of the orientation of membrane protein interactions by varying the binding epitope of the aptamers.[224] This strategy could also be used to investigate the effects of the cell-cycle phase, membrane composition, and drugs and diseases on membrane interactions and dynamics.[224]

The cell membrane and the proteins it contains can sense mechanical forces, and convey this information across the
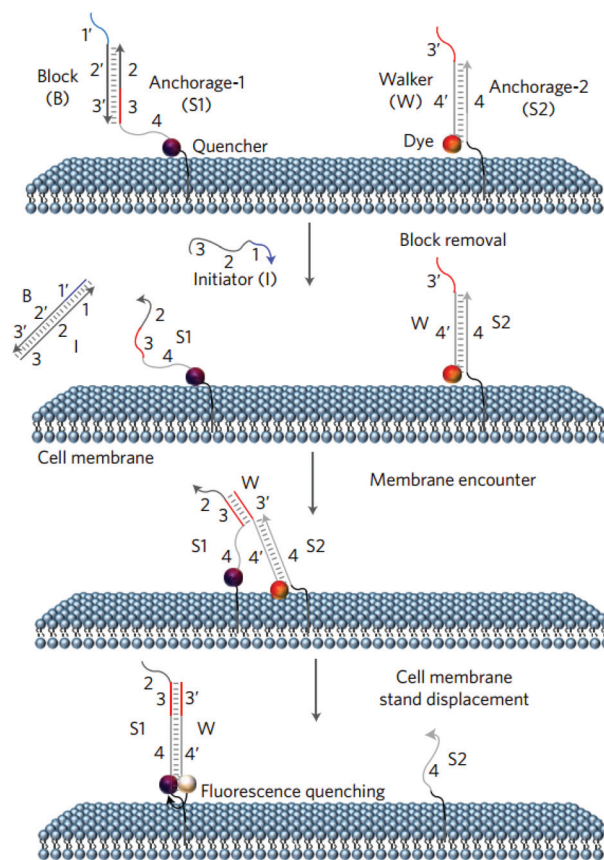
Fig. 25 Strategy for probing interactions on live cell membranes. The initiator (I) displaces the blocking strand (B) from the first anchor strand (S1) to begin the experiment. Subsequent encounters between the anchoring lipid or protein pairs brings the walker strand (W) and the first anchor strand (S1) together and initiates strand displacement. After strand displacement, the fluorescent walker (W) and quencher strand (S1) are hybridised, resulting in a decreased fluorescent signal at a rate which reflects the encounter rate of the two anchoring molecules in the membrane. Adapted with permission from ref. 223. Copyright 2017 Macmillan Publishers Ltd.

membrane to regulate diverse functions. To measure the pico-newton forces applied on the transmembrane protein integrin during adhesion, Zhang *et al.* developed a DNA tension probe with tunable force response thresholds.[225] A surface-anchored strand tagged with a quencher and a fluorescent peptide-displaying strand are bound to the opposite sides of a stem-loop strand (Fig. 26). When cells are plated on a surface, binding of transmembrane integrins to an adhesive peptide exerts tension on the stem-loop which unfolds above a tunable threshold force. Unfolding of the stem-loop produces an increase in the fluorescence signal that is linearly proportional to the number of engaged integrin molecules exceeding the threshold force. The threshold force of the probe can be calibrated experimentally and modulated by the GC content or stability of the stem. The adhesion process can be monitored in real-time with spatial resolution using fluorescence microscopy.
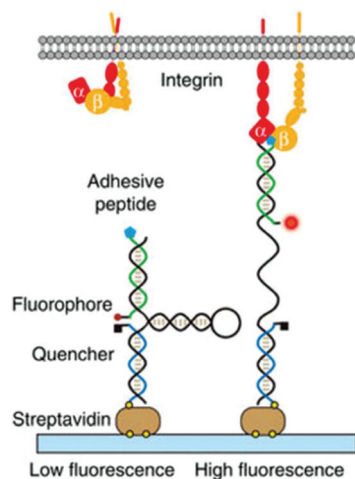
Fig. 26 Schematic of the integrin tension sensor. The sensor is comprised of an anchor strand immobilised onto a surface (blue), a hairpin strand that unfolds under sufficient tension (black) and a ligand strand presenting an adhesive peptide (green). At the opposing termini of the ligand and anchoring strands, a fluorophore and quencher were coupled to report the force-induced unfolding of the hairpin. Adapted with permission from ref. 225. Copyright 2014 Macmillan Publishers Ltd.

Probing interactions between cells and their environment can now be achieved by anchoring DNA switches into plasma membranes. First introduced by Zhao *et al.*, DNA switches that detect proteins in the cell's local microenvironment could serve to elucidate mechanisms of cell-to-cell communication in real-time.[226] In their paper, the authors employed a PDGF-binding aptamer switch that undergoes a conformational change upon PDGF binding, bringing FRET dyes closer in space. This fluorescent switch was covalently anchored to cell membranes, and demonstrated quantitative real-time detection of local changes in the concentration of PDGF secreted by neighbouring cells. Tan *et al.* also developed lipid-functionalised DNA sensors that self-assemble on the cell surface. They used DNAzymes to detect metal ions (Mg^{2+}, Zn^{2+} and Pb^{2+}) (Fig. 27)[227] or G-quadruplexes to quantify K^+ on the cell surface.[228] These cell surface sensors offer new approaches to explore local intercellular signaling processes that may not be captured by analysing the bulk medium.[229]

5. Drug delivery applications

DNA switches can be further engineered to trigger the release of a molecular payload in response to a specific input, such as an abnormal concentration of disease markers. This feature has been extensively exploited by different research teams for a wide variety of drug delivery systems (DDS). Here, we have grouped these DDS into six categories: (1) DNA nanomachines; (2) DNA boxes or containers; (3) microcapsule systems; (4) nanoparticles systems; and (5) nanochannels. The final category of DNA-based DDS employs (6) DNA hydrogels, and will be covered in section 6 of this review.
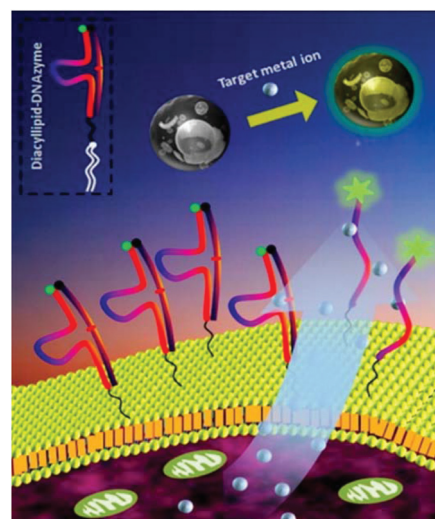
Fig. 27 Schematic representation of the cell membrane-anchored DNAzyme for real-time monitoring of metal ions in the cellular microenvironment. The diacyllipid-DNAzyme self-assembles on the cell surface. Binding of the secreted target metal ion triggers cleavage of the substrate strand by the DNAzyme. The shortened fragments of the cleaved DNA strand dissociate from the duplex, separating the quencher on the substrate strand from the fluorophore on the DNAzyme strand. The fluorescence enhancement is used for metal ion quantification. Reprinted with permission from ref. 227. Copyright 2014 American Chemical Society. Further permissions related to the material should be directed to ACS.

5.1. DNA nanomachines

Due to its unique chemistry and high programmability, DNA represents the ideal material for the construction of stimuli-responsive nanomachines that bear both cargo loading and releasing capabilities. Acidic conditions, often found in the vicinity of tumor cells, are perhaps one of the most common triggers for cargo release.[230,231] This was the inspiration behind Porchetta *et al.*'s work where they proposed a universal strategy for re-engineering aptamers as pH-sensitive molecular transporters. They did so by modifying the cocaine-binding aptamer with a pH-sensitive tail (Fig. 8) that impedes proper folding of the aptamer at low pH, thus forcing the cocaine-bound aptamer to release its cargo.[103] The same research team also reported a similar pH-sensitive DNA nanomachine capable of enzyme-driven cargo loading and enzyme-driven cargo release in response to fluctuations of proton concentrations due to enzymatic activity (*i.e.* pH increases with urease activity and promotes cargo loading; pH decreases with acetylcholinesterase and promote cargo release).[232] More recently, Ricci and Vallée-Bélisle's teams also developed a DNA nanomachine capable of releasing DNA strands directly in serum in the presence of specific antibodies (Fig. 28A and B).[233] In this switch, the binding of the antibody to its epitope induces a steric hindrance effect that triggers the opening of a DNA triplex, which releases the DNA cargo. An important feature of this DNA switch is that it can be modified to bind any desired antibody by only changing the epitope on the switch structure.
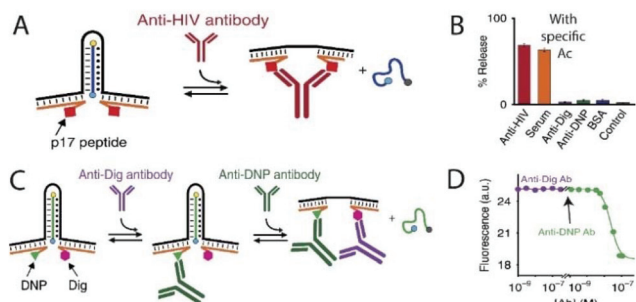
Fig. 28 An antibody-activated drug releasing nanomachines. (A) A DNA nanomachine that releases its payload in presence of specific HIV-antibodies. (B) Specificity of the HIV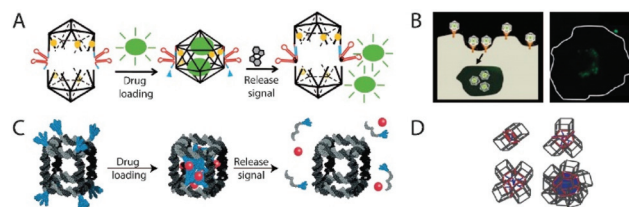-triggered nanomachine. (C) The same nanomachine can also be adapted into a logic gate circuit that requires the successive binding of two specific antibodies (D) to release the molecular payload. Adapted from ref. 233. Published in 2017 by Macmillan Publishers Ltd.

Fig. 29 DNA container switches. (A) A DNA drug-containing capsule with an icosahedron shape employs a cyclic di-GMP binding aptamer to control its opening. (B) DNA capsules are readily internalised by living cells. (C) A DNA box containing DNA switches driven by hydrophobic interactions could be used to load a drug inside the box. (D) Hydrophobic interactions can be used to engineer sophisticated DNA boxes with various applications in drug delivery. Panel A adapted with permission from ref. 239. Copyright 2013 Wiley-VCH. Panel B adapted with permission from ref. 240. Copyright 2011 Macmillan Publishers Ltd. Panel C adapted with permission from ref. 241 Copyright 2013 Macmillan Publishers Ltd. Panel D adapted with permission from ref. 242. Copyright 2016 American Chemical Society. Further permissions related to the material should be directed to ACS.

Moreover, this DDS can be adapted into a logic gate circuit in which a combination of stimuli are needed to produce a response (Fig. 28C and D). Other research teams have taken advantage of the G-quadruplex configuration to build a pH-sensitive DDS that releases proteins in acidic conditions, as has been seen with the thrombin-binding aptamer.[234] Due to its high programmability, DNA nanomachines can be finely tuned to optimise their loading and release behaviour in order to build optimal DDS, as demonstrated in a recent study.[102]

5.2. DNA box switches

DNA is also used as a scaffold to build rationally designed drug containers, such as DNA origami boxes, cubes, nanotubes or icosahedrons,[235–237] that can be opened and closed through a DNA switching mechanism. One advantage of using these containers is that they increase the drug loading capacity (*i.e.* drug/transporter ratio). One of the first examples of such origami switch-based DDS was created by Andersen *et al.*, who built a DNA box with a closing lid whose opening could be triggered with a single DNA strand.[238] A similar cargo release mechanism using a specific DNA strand as a trigger was also adapted in a DNA nanotube containing precisely positioned gold nanoparticles.[243] The versatility of such systems was also demonstrated by Douglas *et al.* with a DDS that could release a payload in the presence of two specific stimuli (*e.g.* cell surface markers) that formed a logic-gate.[244] Similarly, Banerjee *et al.* have re-engineered DNA icosahedrons to release a payload in the presence of cellular messengers like cyclic di-GMP (Fig. 29A).[239] This DDS employs cyclic di-GMP binding aptamers that switch into an open conformation, thus opening the container. Icosahedrons are easily internalised by living cells, which is ideal when building DDS (Fig. 29B).[240] Edwardson *et al.* have designed a protein-inspired DNA cube that comprises a hydrophobic core that can load various hydrophobic drugs (Fig. 29C).[241] Such a DNA cube could be triggered to release its payload in the presence of a specific single-stranded DNA. More recently, Chidchob *et al.* also demonstrated that

this concept of a hydrophobic core could be employed to build DNA-based drug containers of various complex shapes based on hydrophobic interactions (Fig. 29D).[242] Lastly, other DDS made of switching DNA boxes and nanotubes have also been reported by the same research group.[247]

5.3. Microcapsule-based DNA switches

Another strategy to increase DDS drug loading is to use microcapsules made of either organic or inorganic materials that can be readily controlled with DNA switches.[248] For example, Ruiz-Hernandez *et al.* recently adapted cylinders made of mesoporous silica into a container that sequestered a molecular payload that was further capped at each end with magnetic nanoparticles by employing a simple DNA duplex (Fig. 30A).[245] This DDS can be exposed to a specific alternating magnetic field to generate heat that can melt the DNA duplex, and switch the container from a "closed" to an "open" conformation, thus releasing the molecular cargo (Fig. 30A).

Aside from mesoporous silica, various polymers can be used with DNA to form DDS capsules. For example, a calcium carbonate particle can be loaded with a molecular payload, and coated with a positively charged polyelectrolyte that can non-specifically bind DNA to form another coating for the DDS (Fig. 30B).[246] This DNA coating layer contains a DNA switch aptamer that binds to ATP. This binding event induces a conformational change that triggers the disruption of the capsule coating layer, and can release various molecular payloads (*e.g.* quantum dots, microperoxidase or dextran derivatives). Liao *et al.* have also recently used calcium carbonate particles as drug containers that were further coated with a positively charged layer and a negatively charged DNA layer.[249] The DNA layer could undergo a conformational change to form DNA triplex structures when the particle reaches acidic conditions, thus triggering the release of its molecular payload (*e.g.* quantum dots). The same research group also employed
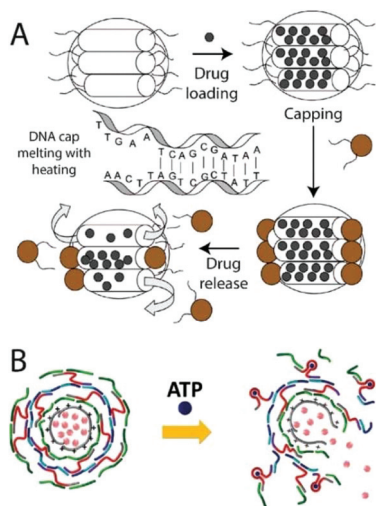
Fig. 30 Microcapsule DNA switches. (A) Closed cylinders of mesoporous silica are capped with magnetic nanoparticles *via* a DNA duplex; heat promotes an open state and the drug payload release. (B) CaCO₃ nanoparticles can be capped with a DNA switch responsive layer that undergoes structure switching in the presence of ATP, which induces drug release. Panel A adapted with permission from ref. 245.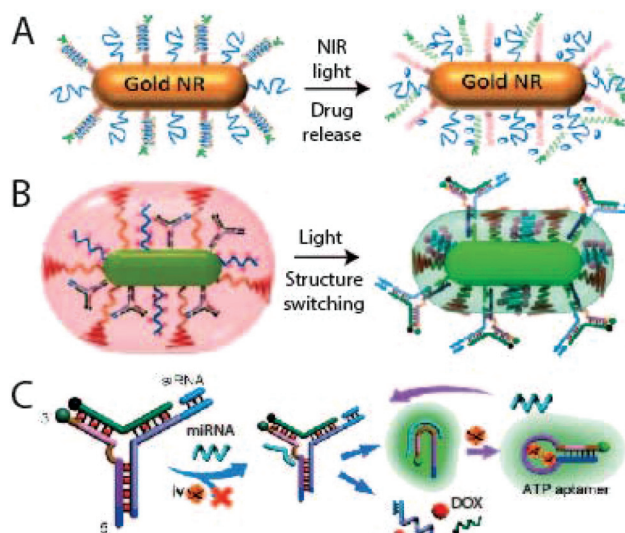 Copyright 2011 American Chemical Society. Panel B adapted with permission from ref. 246 Copyright 2015 American Chemical Society.

Fig. 31 Nanoparticles DNA switches. (A) Doxorubicin (DOX) was loaded on DNA-attached sequences on the surface of gold nanorods. Heat generated following light irradiation causes the melting of the DNA switches and the release of DOX. (B) A gold nanorod undergoes a light-dependent structure switching of its coating surface that exposed DNA switches (C) that in turn can release their payloads. Panel A adapted from ref. 250. Copyright 2012 Wiley-VCH. Panels B and C adapted with permission from ref. 251. Copyright 2016 American Chemical Society.

metal–organic frameworks that formed a drug container that could be capped with DNA switches forming i-motif structures giving a "CLOSED" state in an acidic environment.[252] This DNA switch can then switch to an "OPEN" state in a neutral pH, and then induce drug release from the DDS.

5.4. Nanoparticle-based DNA switches

Gold nanoparticles are a versatile class of material to which DNA switches can be easily anchored using simple chemistry (*e.g. via* a thiol–gold bond) to build stimuli-responsive DDS. A meaningful example was reported by Xiao *et al.*, who have attached various DNA switches transporting doxorubicin (DOX) on the surface of gold nanorods (Fig. 31A).[250] Upon irradiating with near-infrared light, the nanoparicle heats and causes the opening of the DNA switch, and thus the release of the DOX payload. A similar DDS was reported by Song *et al.* who also used gold nanoparticles to attach at their surface pH-responsive DNA switches loaded with DOX.[253] A decrease of pH induces the folding of the surface-bound DNA switch to an i-motif, triggering the release of the loaded DOX.

More recently, Zhang *et al.* developed a sophisticated stimuli-responsive and thermosensitive DDS with a signal amplification mechanism.[251] This DDS is a polyethylene glycol (PEG) protected gold nanorod whose surface contains various DNA switches and a peptide motif for targeting, loading and delivery purposes (Fig. 31B). Due to the enhanced permeability and retention effect of cancer tissue, this DDS accumulates at the tumor site where it can be activated by light irradiation to remove the protecting PEG layer. This allows exposure of the DNA switches and peptide motif, the latter promoting DDS

internalisation by the tumor cells. Once inside the cell, the DNA switches can be activated with endogenous miRNA that induces a toehold-mediated conformational change (Fig. 31C), which in turn releases the loaded therapeutic agents, DOX and small interfering RNA (siRNA), as well as the ATP aptamer. The DDS amplification mechanism comes from this ATP aptamer that releases the initial miRNA trigger upon binding of ATP; this microRNA is then free to activate other DNA switches.

5.5. DNA nanochannels

DNA nanochannels or nanopores could find tremendous applications in drug delivery by allowing the direct and selective transport of drugs directly inside living cells.[254] One of the earliest examples of stimuli-responsive nanochannels was reported by Hou *et al.* where they grafted G-quadruplex DNA switches on an artificial nanopore that could undergo structure switching from a random coil to a G-quadruplex organised structure in the presence of surrounding K⁺ ions, which successfully decreases the diameter of the nanopore.[255] Addition of single-stranded DNA to the nanopore allows DNA duplex formation that further reduces the pore diameter to a "closed state". The same research group also later reported the use of a photo-reactive DNA switch containing azobenzene that could undergo *cis* to *trans* isomerisation, which triggers a change in channel diameter from a closed state to a loose open state.[256] Following this, Burns *et al.* engineered concatenated DNA strands to precisely assemble as a channel comprising hydrophobic patches for insertion into a lipid bilayer (Fig. 32A).[257] This DNA structure employed a "lock" DNA
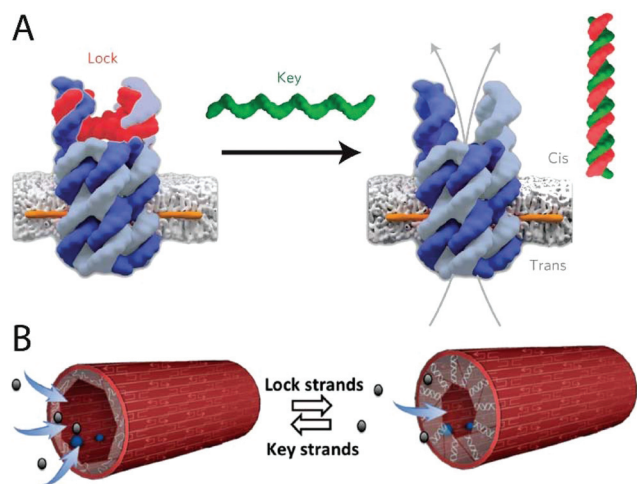
Fig. 32 DNA nanochannels. (A) A DNA nanochannel spanning a lipid bilayer can be opened and closed with a DNA switch that either blocks or allows the drug to pass through the channel. (B) A similar nanogate built with DNA origami could be triggered to an open or closed state depending on the DNA switch used. Panal A adapted with permission from ref. 257. Copyright 2016 Macmillan Publishers Ltd. Panel B adapted with permission from ref. 258. Copyright 2016 The Royal Society of Chemsitry.

Fig. 33 Light–activated DNA-based hydrogels reversibly change their volume in response to UV or visible light. Reprinted with permission from ref. 263. Copyright 2012 American Chemical Society.

switch that maintains the channel closed but that could be reverted to an "open" state by the addition of a "key" single-stranded DNA. DNA origami has also been employed by researchers, such as Wang et al., to build DNA nanochannels whose diameter can be altered in an open or closed state with the help of "lock" and "key" DNA switches that either close or open the channel, respectively (Fig. 32B).[258]

6. Switchable DNA hydrogels

Hydrogels are a class of functional materials that contain highly cross-linked hydrophilic polymer networks that can swell in size after absorb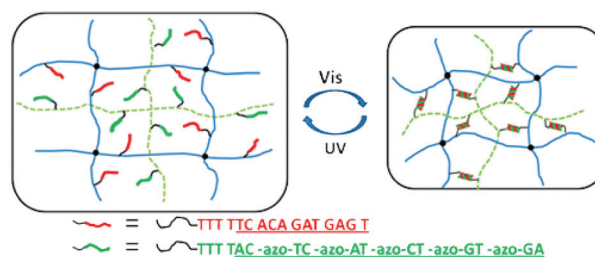ing water. Within this domain, there are also stimuli-responsive hydrogels that rely on chemical or physical triggers to undergo reversible state transitions from hydrogel-to-solution or hydrogel-to-solid. In recent years, various switching hydrogels have been developed that incorporate DNA switches to respond to a variety of input signals. Pure DNA hydrogels are made entirely from DNA, whereas hybrid DNA hydrogels often use DNA as a responsive component. Typically, they involve the tethering of acrydite-functionalised nucleic acids with a polymer chain, such as polyacrylamide. Various types of inputs can be used to induce DNA structural changes, including light, temperature, pH, metal ions, small molecules or proteins.[259–262] Here, we discuss recent advances involving switchable DNA hydrogels.

6.1. Shape-changing gels

Bridging the fields of materials science and bionanotechnology, smart DNA hydrogels can alter their properties in

response to specific chemical or physical stimuli. As such, conformational changes of DNA at the nanoscale often result in observable changes at the macroscale.[259,261] One example is by Peng et al. who have reported a reversible volume-changing hydrogel that employs a light-induced azobenzene DNA switch.[263] Under visible light, two complementary ssDNA attached to the gel matrix hybridise with each other and create extra-crosslinks in the polymer network, thus reducing the hydrogel volume (Fig. 33). In presence of UV-light, the azobenzene groups on one of the ssDNA adopts a cis-isomer conformation, which destabilises the DNA duplex and triggers gel relaxation in a reversible manner.

Another example is by Hu et al. who have developed DNA hydrogels possessing pH-sensitive shape-memory properties (Fig. 34). Their design employs the programmable "triplex" pH-sensitive switch (1) discussed in Fig. 8.[129] The acrydite-triplex switch is closed at pH 5, but opens up at pH 7, liberating a ssDNA sequence (I) complementary to the acrydite-ssDNA-2. The hydrogel mixture is first heated at pH 7, and placed in a triangle-shaped mould. Cooling and removal from the mould allowed for the formation of a triangle-shaped hydrogel that is stabilised by the duplex formed between the triplex switch-1 and the ssDNA-2, as well as by the self-complementary ssDNA-3. Upon reducing the pH to 5, the triplex switch-1 dissociates from the ssDNA-2, and adopts a closed conformation driving the hydrogel to a shapeless quasi-liquid phase (Fig. 34B). The (3)–(3) duplexes maintain a dictated spatial structural entanglement of the polymer chains; in other words, it internally-stores the memory of the hydrogel shape. Upon returning to neutral pH conditions, the hydrogel resumes its well-defined triangle shape. The pH sensitivity of this hydrogel can also be programmed to cover different pH ranges by modifying the C–G·C/T–A·T ratio of the triplex switch.[264,265]

Further recent works conducted by Lu et al. have explored multiple triggers for shape-memory DNA hydrogels, such as incorporation of K^+-stabilised G-quadruplex units,[266] along with a pH and Ag^+ ions-stabilised i-motif.[267] Hu et al. have also recently reported an asymmetrical bilayer hybrid DNA-based hydrogel capable of mechanical bending changes (transitioning between a stiff bent structure to a more relaxed linear structure) in response to various triggers.[268] The triggers

Fig. 34 pH-sensitive shape-memory hydrogels. (A) The hydrogel is made from acrydite-modified pH 'triplex' switch-(1), DNA strands (2), self-complementary DNA strand (3) and polyacrylamide. It is formed using a triangle-shape mould at pH 7. (B) Illustration of the pH-triggered reversible transition from the triangle-shaped hydrogel at pH 7 and the quasi-liquid state at pH 5. The design is based on a duplex nucleic acid (permanent memory) and C−G·C+ triplex crosslinking units. (C) Cycling of the pH-triggered shape transition. Adapted with permission from ref. 264. Copyright 2015 Wiley-VCH.

used therein included temperature- and pH-controlled formation/destabilisation of the i-motif, as well as K+ ion and crown ether formation/destabilisation of G-quadruplexes. Additionally, they demonstrated that enzymes incorporated into the hydrogel enabled biocatalytic control of the shape structure, wherein glucose oxidase acidifies the system via catalysis of glucose (bent structure), and urease neutralises the system during its catalysis of urea (linear structure).

6.2. Biosensor gels

Hydrogels can also be adapted in convenient biosensors. Zhang et al., for example, have developed a DNA hydrogel for visual and fluorometric detection of thrombin (Fig. 35).[269] The hydrogel biosensor undergoes a target responsive gel-to-solution transition. First, the DNA hydrogel is formed by crosslinking the complementary segments of a Y-shaped DNA and a linker DNA containing the thrombin aptamer sequence. The hydrogel bottom layer encapsulates 13 nm gold nanoparticles that are unable to mix with the upper layer of buffer. Binding of thrombin by the linker DNA collapses and dissolves the hydrogel, thus releasing gold nanoparticles into the buffer for visual detection. Thrombin can then be quantified based on FRET between negatively charged gold nanoparticles and positively charged polyethyleneimine (PEI)-functionalised CdTe

Fig. 35 Hydrogel-based biosensor. The Y-shaped DNA (Y-DNA) and the linker DNA-containing aptamer (L-DNA) form a DNA hydrogel that encapsulates gold nanoparticles. Addition of thrombin collapses and dissolves the hydrogel, releasing the nanoparticles into the buffer layer for visual detection. The protein can be quantified via FRET between the Au nanoparticles and CdTe quantum dots. Reprinted with permission from ref. 269. Copyright 2013 American Chemical Society.

quantum dots (QDs). Additionally, the biosensing system works in serum.[269]

6.3. Drug delivery gels

Hydrogels have attracted much interest as water soluble polymers that could be used to transport drugs safely into a living organism. One such example was reported by Kang et al., where a light-sensitive hydrogel, bearing an azobenzene group, enables the release of a molecular payload upon UV irradiation.[270] Recently, Song et al. built a similar DDS that employs a hydrogel loaded with DNA strands, doxorubicin and gold nanoparticles (Fig. 36).[271] The nanoparticles could then be excited at their plasmon resonance with light irradiation, which generates heat that induces the opening of the DNA switch, thereby causing the release of the doxorubicin payload. More recently, Li et al. have reported a hydrogel whose formation was driven by the folding of multiplex aligned G-quadruplex DNA switches bearing reactive groups like iminoboronate bonds that allowed the DNA switch to react with ligands like glucose.[272] The presence of either glucose or a pH decrease could trigger the switching of the G-quadruplex

Fig. 36 A hydrogel DDS. This system comprises a DNA switch loaded with doxorubicin whose release can be triggered by light irradiation of surrounding gold nanoparticles. Adapted with permission from ref. 271. Copyright 2015 The Royal Society of Chemistry.

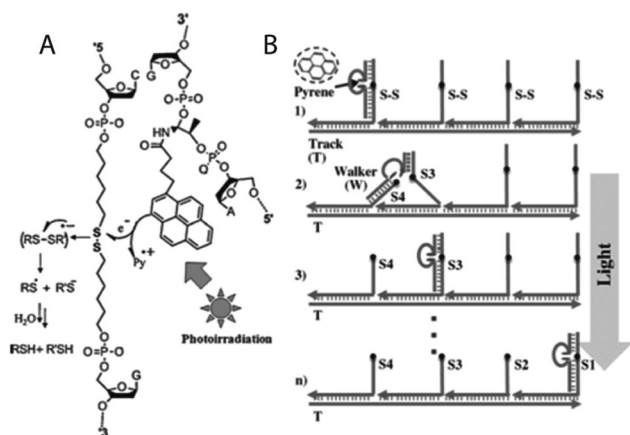to a disordered state that melted the hydrogel, and resulted in the release of its molecular payload.

7. DNA walkers, logic circuits, and chemical synthesis platforms

Drawing upon the structural and functional programmability of DNA switches, well-controlled molecular devices that can perform specific tasks have been developed recently such as DNA walkers, logic gates, nanomachines for molecular synthesis, as well as other noteworthy devices.[273,274]

7.1. DNA walkers

Inspired by biological protein motors that move autonomously along a track, DNA-based molecular walkers play an important role in the development of nanotechnology. DNA walkers typically transform chemical or light energy into kinetic movement similarly to how protein motors use ATP hydrolysis or the transmembrane ionic gradient to produce kinetic motion.[275] They have been utilised in several applications including biosensing, biocomputing, material assembly,[276] payload transport and release,[277] as well as DNA walker-mediated organic synthesis.[278] This class of DNA-based device has now been engineered to move along linear, 2D and 3D tracks, and its trigger mechanism generally involves strand displacement, binding-induced conformational change, or enzyme-based DNA cleavage.[273]

Using strand displacement mechanisms, You *et al.* designed a DNA walker system composed of a ssDNA track (T), four anchorage sites (S1–S4) and a light sensitive walker (W) (Fig. 37).[279] Two DNA walking legs of uneven length, linked by a pyrene moiety, are hybridised to an anchor segment that contains an internal disulfide bond. Upon irradiation at

350 nm, pyrene assisted-photolysis of the disulfide bond occurs and initiates the walking movement (Fig. 37A). While the longer leg remains bound to the first anchor segment, the shorter one hybridises with the next anchor, which triggers a toehold-mediated strand displacement to bring the walker to the second anchor segment.

Another example is by Wang *et al.*, who demonstrated a reversible "bipedal stepper" system, which employs a binding-induced conformational change triggered by small molecules (Fig. 38).[280] Here, the track consists of four footholds, each containing a complementary strand with a sticky end bearing a specific fluorophore (F_1–F_4). The walker consists of two arms (green and purple) tied together by a blocker strand (grey) bearing a quencher (Q) at both extremities. The walker's forward motion, from Panel A to B, is triggered by Hg^{2+} *via* T–Hg^{2+}–T formation, and, from Panel B to C, by H^+ *via* an i-motif structure. This can be reversed through disruption of these interactions by cysteine and OH^-, respectively, leading to the walkers's backward motion. Finally, fluorescence analysis allows monitoring of the walker's location as reflected by the quenching of specific fluorophores.

A molecular spider was created by Lund *et al.* based on enzymatic reactions.[281] The spider is made of a streptavidin molecule attached with three DNA enzyme catalytic legs and a starting DNA strand. The landscape on which this spider moves consists of a rectangular DNA-origami made from a 7 249-nucleotide DNA strand and 202 distinct staple strands. The spider is first positioned at the start of the track using the starting DNA strand. A higher affinity strand is used to trigger the release of the spider along the track. Legs of the spider then bind to neighbouring complementary sequences that are on top of the origami landscape. The walking process is triggered by the cleavage of the complementary sequence (sub-
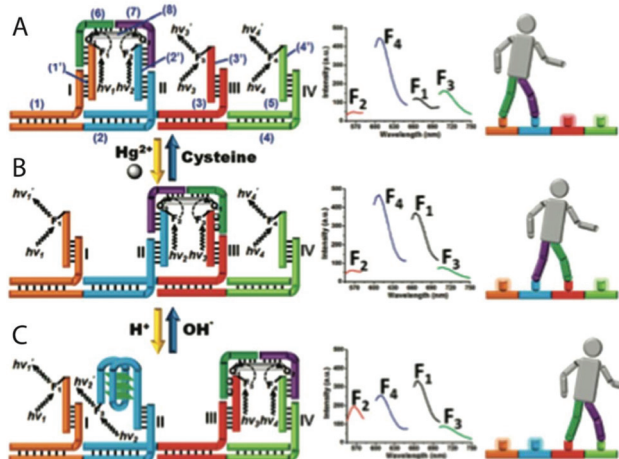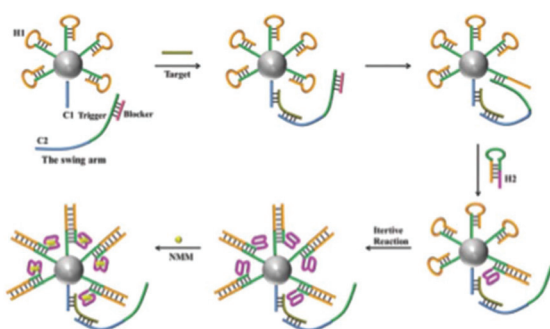

Fig. 37 A DNA walker system based on photolysis. (A) Pyrene-assisted photolysis of the disulfide bond within DNA structures. (B) The walking system includes a track, four anchorage sites and the walker. Light-triggered photolysis provides energy for the walking, which uses a toehold-mediated strand displacement mechanism. Adapted with permission from ref. 279. Copyright 2012 Wiley-VCH.

Fig. 38 A bipedal walker responsive to Hg^{2+}/cysteine and H^+/OH^- as triggers. (A) The walker immobilised on foothold I and II quenches fluorescence from F1 and F2 but not from F3 and F4, as illustred by the fluorescence spectrum. (B–C) Moving of the walker along the track with the corresponding fluorescence spectrum. Adapted with permission from ref. 280. Copyright 2011 American Chemical Society.

strate) by the DNA enzymatic leg, and leaves a shorter strand as the product. The legs then start moving randomly. Because the products are shorter, the dissociation rates of the legs are on average faster, whereas the legs will stay longer with substrate. This ensures that the body of the molecular spider moves toward substrate-rich regions, thus decreasing the chance of the spider to walk backward.[281] Yang *et al.* have developed a similar approach to move DNA on gold nanoparticules.[277]

More recently, DNA walkers have also been adapted as efficient biosensors (Fig. 39). Taking advantage of the high amplification capacity of 3D tracks (higher surface area), Li *et al.* have developed a highly sensitive (LOD: 4.1 fM) fluorescent DNA sensor using magnetic nanobeads.[282] The track on the nanobeads consists of many anchored hairpins (H1) and one ligand capturing oligonucleotide (C1). The system also requires a "swing arm" made from a ligand captured oligonucleotide (C2), a trigger oligonucleotide and a blocker DNA. The blocker partially hybridises with the swing arm in order to minimise its interaction with the anchored hairpin H1 in the absence of the DNA target. Another strand, the signaling hairpin (H2) contains a G-quadruplex and provides a fluorescent output in presence of N-methyl mesoporphyrin IX (NMM). In presence of target DNA, the swing arm hybridises to the C1 sequence on the nanobead, and activates the opening of an anchored hairpin (H1) due to proximity. Once opened, H1 then hybridises to H2, which brings a G-quadruplex onto the nanobead and releases the swing arm. The latter is now available for another activation cycle. Such a walking mechanism allows several G-quadruplex structures to be brought on the nanobead using only one target DNA, resulting therefore in signal amplification.

7.2. DNA logic circuits

Computation based on the technology we know so far is starting to end its exponential development due to limitations on miniaturisation of components and their inherent speed.[283] To solve this problem, researchers have started to explore new scientific avenues such as quantum computing, and the more biologically-inspired molecular computing. The latter field is influenced by the power of natural biological systems used by cells to communicate and treat information.[283] The first demonstration of artificial molecular computing was designed by Adleman, which was able to resolve a Hamiltonian path of 7 vertexes.[284] It was only after the remarkable work of Seeman and others that the field of DNA computing truly began to emerge.[285] Over the years, research groups have used DNA switches to create logic circuits that can, for example, play games against humans,[286–289] calculate the square root of four-bit binary numbers,[290] act as keypad-lock security systems,[291] perform cancer theranostics,[292–294] and carry out molecular diagnostics.[295–297] In the following passages, we will discuss two recent articles that, we believe, provide an effective overview of the impact of DNA logic circuits for future applications.
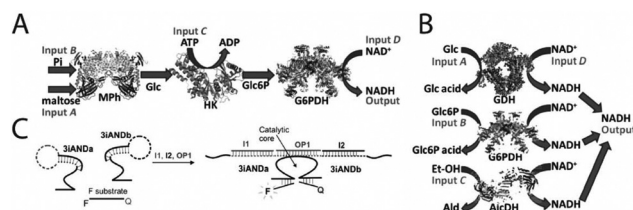
Antibodies are crucial molecular recognition tools in the life sciences and are an important class of drugs. New strategies are currently being sought to regulate their activity, thereby allowing the antibody to be active only when needed. Recently, Janssen *et al.* developed a non-covalent approach to block antigen binding sites by employing a dsDNA-based bivalent ligand (Fig. 40A).[298] They showed that a rigid dsDNA can block the antibody in a 1 : 1 ratio. By introducing a toehold sequence in this dsDNA linker, Janssen *et al.* were able to introduce a logic response for "unlocking" the antibody.[299]
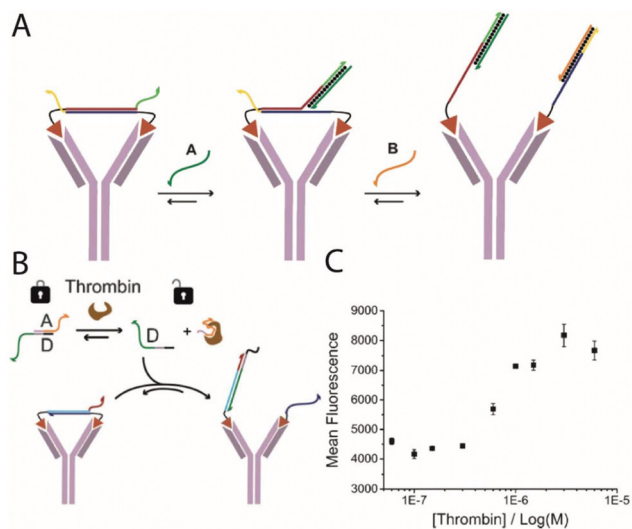
Fig. 40 Activable antibodies using a DNA-based logic gate. (A) A dsDNA containing two ligands and two toehold sequences occupies the antigen binding sites on the antibody. Addition of input DNA strands A and B can lead to a logic OR- or an AND-gate depending on the length of the overlapping sequences. (B) A similar design can be employed to create a protein-based aptamer logic circuit. In this design, the input DNA strand is sequestered by an aptamer into a duplex. When the ligand of the aptamer is present (thrombin in this case), the strand is released and the antibody is reactivated as revealed by the increased fluorescence (C). Adapted with permission from ref. 299. Copyright 2015 Wiley-VCH.

Fig. 39 A fluorescent biosensor that uses a DNA walker system. The walking mechanism enables signal amplification by bringing many G-quadruplex structures (which can bind the fluorescent NMM) on the nanobead using only one target DNA. Reprinted with permission from ref. 282. Copyright 2017 The Royal Society of Chemistry.

When adding DNA strands to produce strand displacement, two DNA-monovalent ligands, with lower affinity toward the antibody, are created, therefore resulting in their dissociation and activation of the antibody. A logic response can also be engineered by employing two different toehold sequences introduced inside the dsDNA-bivalent ligand (Fig. 40A). This approach could be further adapted for activation by proteins using aptamers (Fig. 40B and C). The authors showed that their antibody could be activated in presence of two biomolecules (AND-gate), or only when one of the two molecules is present (OR-gate).

Mailloux *et al.* have designed an electrochemical interface that couples a DNA-based and an enzyme-based logic gate (Fig. 41).[300] In their system, two different enzymatic logic gates are designed to produce NADH as the output. The first logic gate is a three concatenated Boolean AND-gate that produces a response only when the four inputs (maltose, Pi, ATP and NAD^+) are present (Fig. 41A). The second logic gate is a three-input OR-gate connected to an AND-gate that produces an output only if NAD^+ is present with any of three inputs: glucose, glucose-6-phosphate and ethanol (Fig. 41B). When NADH is produced by one of these two circuits, its oxidation occurs at the surface of the anodic electrode, and reduction of Fe^{+3} to Fe^{2+} takes place on the surface of the cathodic electrode. The reduction of Fe^{3+} leads to the dissolution of a Fe^{3+}-cross-linked alginate film, and the release of the film's encapsulated DNA strand. This interface enables communication between the enzymatic logic gate and the three-input deoxyribozyme AND-gate logic circuit (Fig. 41C). This work demonstrates the possibility to create "universal" logic gate interfaces made of enzymes and DNA switch parts, which possess massive parallel data processing.
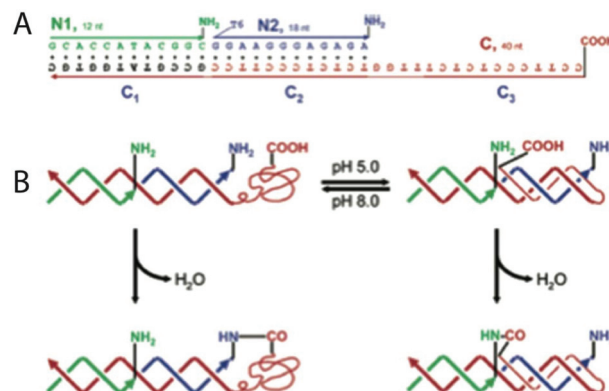
7.3. Organic synthesis using DNA switches

Control over chemical reactivity (*i.e.* stereoselectivity) is a major challenge in organic synthesis. The programmability and diversity of nucleic acids provide an interesting solution to overcome this challenge. Recent developments of DNA-assisted organic synthesis range from switchable DNA structures acting as stereocontrol elements to DNA encoded reactions (DNA template reactions).[301]

Several researchers have shown that DNA can act as a stereocontrol element to provide a chiral environment.[301–305] Wang *et al.*, however, recently demonstrated that the catalytic activity of such DNA structures can be switched "on-the-fly" by stabilising an alternative conformation.[305] They found that a G-quadruplex structure can catalyse Diels–Alder reactions and increase the enantiomeric excess (ee) of the *endo* isomer from 0% to 17%. This ee can be further increased when this G-quadruplex switches to an alternative antiparallel conformation through a Cu^{2+}-induced conformational change. Adding Na^+ cation, which further stabilises this antiparallel structure, and increases enantioselectivity by up to 74% ee. In contrast, addition of PEG200, which stabilises the parallel conformation, favours the formation of the opposite enantiomer.[305]

Chen and Mao, have also developed a pH-sensitive DNA scaffold that can be reprogrammed *via* pH change to perform distinct chemical reactions (Fig. 42).[306] This platform is composed of a scaffold ssDNA subdivided in three sections (C1, C2 and C3) to which two amine group-functionalised ssDNA (N1 and N2) can be hybridised (on complementary sequences C1 and C2, respectively). The C3 segment, on the other hand, is conjugated with a carboxylic acid. At pH 5, a triple helix structure forms between the segment C3 and the

Fig. 41 An electrochemical DNA- and enzyme-based logic gate. (A) A first enzymatic logic circuit is composed of three enzymes that produce a three concatenated Boolean AND gate. The output is triggered by the presence of Pi, maltose, ATP and NAD^+ using the enzymes maltose phosphorylase (MPh), hexokinase (HK) and glucose-6-phosphate dehydrogenase (G6PDH). (B) A second enzymatic logic circuit is composed of three NAP^+ dependant enzymes. The output is triggered by the presence of NAD^+ and either glucose, glucose-6-phosphate or ethanol using the enzymes glucose dehydrogenase (GDH), G6PDH and alcohol dehydrogenase (AlcDH). (C) The DNA logic gate is based on a three-input deoxyribozyme AND gate (3iAND). The output is triggered by the presence of three DNA strands, two are already in the system (I1 and I2) and the other one is released in response to the enzymatic logic circuit. In absence of input, the gate is dissociated. In presence of the input, the gate is formed and reveals a catalytic core that cleaves a fluorophore–quencher reporter DNA strand. An increase of fluorescence shows the activity of the gate0. Adapted with permission from ref. 300. Copyright 2015 Wiley-VCH.

Fig. 42 A pH switching DNA-based assisted chemical reaction. (A) DNA scaffold and reactants. (B) Changing pH triggers a conformational change that moves the carboxylic group of the C segment either closer to N1 or N2, thus generating the C–N1 or C–N2 molecules, respectively. Adapted with permission from ref. 306. Copyright 2004 American Chemical Society.

C2-N2 *via* formation of C⁺G–C triplets. The carboxylic group on C3 is therefore brought next to the amino group on N1, triggering the amide bond between C and N1. However, at pH 8, C3 adopts a random coil conformation, and the carboxylic group on C reacts instead with the amino group on N2.

DNA walkers have also been employed to direct chemical synthesis using DNA templates. He and Liu, for example, have designed a DNAzyme walker (W) on which several specific chemical groups can be sequentially added through a series of amine acylation reactions taking place along the walker's path (Fig. 43).[278] This DNA-based "ribosome mimetic" system contains a ssDNA track (called T) with an initiation site I and three codon sites, C1, C2, C3, that can bind substrates S1, S2, S3, respectively. The substrates' overall structures are similar to tRNA, and contain a small molecule building block followed by a docking region, D1, containing two consecutive central RNA nucleotides, a second docking region, D2, and a 21 unique "anticodons" nucleotide sequence complementary to template codons C1, C2, and C3. In solution, the substrates spontaneously bind the DNA template, and the reaction is initiated by adding an initiator DNA, S0, which bring the DNAzyme walker strand onto the DNA template. The DNA walker then hybridises to the first substrate through its D1 sequence, which favours its translocation from S0 to S1. The DNA template reaction occurs between an amine group on the walker (W) and an NHS ester group on S1, and the first amino building block is added to the walker. After cleavage of the ribonucleotide on S1 by the DNAzyme walker, the latter will spontaneously move to the higher affinity substrate S2, which

will lead to the addition of a second amino building block on the walker. This cycle can be repeated many times to create an impressive and programmable one-pot reaction without undesired side products.[278]

8. Conclusions

Throughout this review article, we have presented a summary of various design strategies employed to engineer efficient programmable DNA switches for a wide variety of applications. Designing DNA switches requires careful consideration of various interconnected factors, including the nature of the desired input, its structure switching mechanism, as well as its desired function and response. DNA switches can be activated by a wide range of stimuli, from temperature and light, to chemical stimuli such as protons, ions, small molecules, nucleic acids, and proteins. They can serve as efficient biosensors for various environmental and medical applications, and can also be employed to probe complex biochemical mechanisms, such as gene expression, single molecule movement inside cells, and membrane-associated processes. Beyond bioanalytical detection, DNA switches can be readily adapted into efficient drug delivery systems (DDS) of various natures, sizes and loading efficiencies (*e.g.* switchable transporters, switchable DNA containers, switchable microcapsules, nanoparticles and nanochannels). DNA switches can also be adapted in structure-switching hydrogels that change their shape in response to a wide range of molecular inputs. These hydrogels can act as convenient biosensors or DDS. DNA switches can also serve as building blocks for more complex nanosystems, such as DNA walkers that can transport (sometimes in a reversible manner) various payloads on defined 1D, 2D or 3D pathways in response to different input molecules. They can be engineered into logic gates that analyse complex molecular mixtures and react *via* a specific function in a programmed, quantitative manner. Finally, DNA switches are also increasingly applied in the field of organic synthesis to create, among other strategies, elaborate one-pot efficient synthesis reactions.

Programmable DNA switches are likely to drive many innovations in the fields of medicine, green chemistry, and nanotechnology, but several challenges lie ahead before realising this promise beyond laboratory-scale prototypes.[307] One such challenge is developing switches that achieve sufficient specificity and selectivity (*i.e.* only triggered by a specific molecular input) even in complex conditions or environments (such as whole blood, soil, *etc.*). To that end, we believe that expending the DNA code with other artificial nucleotides should greatly contribute to creating more specific recognition elements.[29,30] Another challenge consists of better characterising and optimising DNA switch systems to obtain their innate structural and dynamic profiles. Such information would provide the rational basis to better optimise the switch's function and response behaviour. With this in mind, we believe that novel tools to characterise the switch's thermodynamic signature
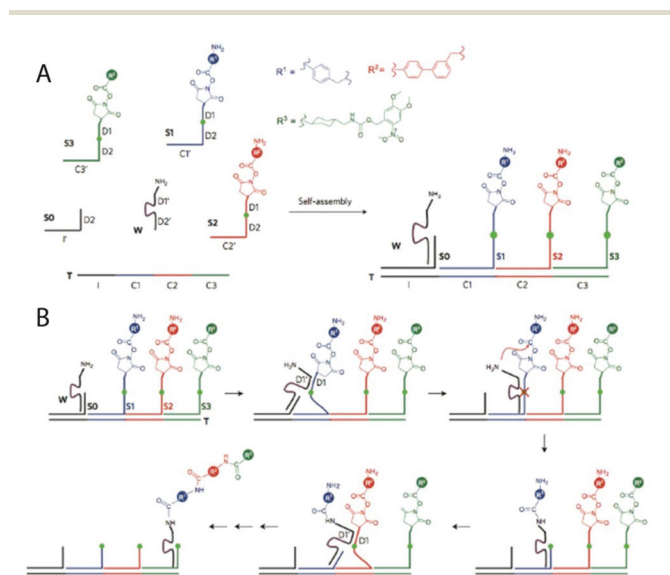
Fig. 43 DNA walker-assisted chemical reactions. (A) This DNA-based "ribosome mimetic" system is composed of a ssDNA track, T, (mimicking mRNA) with an initiation site I and three codon sites (C1, C2, C3) that can bind the substrates (S1, S2, S3, respectively). The DNA walker, W, is a DNAzyme on which many building blocks can be attached though various cycles of amine acylation reactions. (B) Details of the multistep synthesis. Adapted with permission from ref. 278. Copyright 2010 Macmillan Publishers Ltd.

(see ref. 46) and tune it, using simple and inexpensive strategies (such as employing inhibitors or activators[90]), should greatly contribute to making design strategies more rational and quantitative. Concerning switch kinetics, it is also important to note that activation and deactivation of DNA switches using a DNA trigger remains relatively slow, which limits applications such as DNA computing. More specific challenges to move beyond laboratory-scale prototypes include optimising the accuracy (through calibration against a standard), stability, repeatability, and reproducibility of DNA switch systems.[307] *In vivo* applications will also require a better understanding of the mechanisms underlying intracellular uptake, trafficking, and nanotoxicology,[308] in addition to the characterisation of their pharmacokinetic properties. Finally, a better understanding of large-scale production of DNA-based systems for better yields and lower costs[309] is mandatory to scale-up laboratory or pilot technologies to reach the production and commercialisation stages.

Conflicts of interest

The authors declare no conflict of interest.

Acknowledgements

Notes and references

1 Y. Krishnan and F. C. Simmel, *Angew. Chem., Int. Ed.*, 2011, **50**, 3124–3156.
2 F. Wang, X. Liu and I. Willner, *Angew. Chem., Int. Ed.*, 2015, **54**, 1098–1129.
3 G. Ke, C. Wang, Y. Ge, N. Zheng, Z. Zhu and C. J. Yang, *J. Am. Chem. Soc.*, 2012, **134**, 18908–18911.
4 A. T. Jonstrup, J. Fredsøe and A. H. Andersen, *Sensors*, 2013, **13**, 5937–5944.
5 S. Ebrahimi, Y. Akhlaghi, M. Kompany-Zareh and Å. Rinnan, *ACS Nano*, 2014, **8**, 10372–10382.
6 D. Gareau, A. Desrosiers and A. Vallée-Bélisle, *Nano Lett.*, 2016, **16**, 3976–3981.
7 Y. Wu, J. Liu, Y. Wang, K. Li, L. Li, J. Xu and D. Wu, *ACS Appl. Mater. Interfaces*, 2017, **9**, 11073–11081.
8 H. Asanuma, T. Ito, T. Yoshida, X. Liang and M. Komiyama, *Angew. Chem., Int. Ed.*, 1999, **38**, 2393–2395.
9 C. Dohno and K. Nakatani, *Chem. Soc. Rev.*, 2011, **40**, 5718–5729.
10 B. Y. Won, C. Jung, K. S. Park and H. G. Park, *Electrochem. Commun.*, 2013, **27**, 100–103.
11 D. Sen and W. Gilbert, *Nature*, 1990, **344**, 410.
12 Z. Lin, Y. Chen, X. Li and W. Fang, *Analyst*, 2011, **136**, 2367–2372.
13 M. Hoang, P.-J. J. Huang and J. Liu, *ACS Sens.*, 2015, **1**, 137–143.
14 D. Bhattacharyya, G. M. Arachchilage and S. Basu, *Front. Chem.*, 2016, **4**, 38.
15 Y. Miyake, H. Togashi, M. Tashiro, H. Yamaguchi, S. Oda, M. Kudo, Y. Tanaka, Y. Kondo, R. Sawa, T. Fujimoto, T. Machinami and A. Ono, *J. Am. Chem. Soc.*, 2006, **128**, 2172–2173.
16 K. S. Park and H. G. Park, *Curr. Opin. Biotechnol.*, 2014, **28**, 17–24.
17 A. Ono, S. Cao, H. Togashi, M. Tashiro, T. Fujimoto, T. Machinami, S. Oda, Y. Miyake, I. Okamoto and Y. Tanaka, *Chem. Commun.*, 2008, 4825–4827.
18 H. A. Day, P. Pavlou and Z. A. Waller, *Bioorg. Med. Chem.*, 2014, **22**, 4407–4418.
19 A. Dembska, *Anal. Chim. Acta*, 2016, **930**, 1–12.
20 Y. Dong, Z. Yang and D. Liu, *Acc. Chem. Res.*, 2014, **47**, 1853–1860.
21 Y. Hu, A. Cecconello, A. Idili, F. Ricci and I. Willner, *Angew. Chem.*, 2017, **56**, 15210–15233.
22 F. Pfeiffer and G. Mayer, *Front. Chem.*, 2016, **4**, 25.
23 N. Hamaguchi, A. Ellington and M. Stanton, *Anal. Biochem.*, 2001, **294**, 126–131.
24 P. K. R. Kumar, *Biosensors*, 2016, **6**, 40.
25 A. Davydova, M. Vorobjeva, D. Pyshnyi, S. Altman, V. Vlassov and A. Venyaminova, *Crit. Rev. Microbiol.*, 2016, **42**, 847–865.
26 B. Deng, Y. Lin, C. Wang, F. Li, Z. Wang, H. Zhang, X.-F. Li and X. C. Le, *Anal. Chim. Acta*, 2014, **837**, 1–15.
27 C. Tuerk and L. Gold, *Science*, 1990, **249**, 505–510.
28 M. Darmostuk, S. Rimpelova, H. Gbelcova and T. Ruml, *Biotechnol. Adv.*, 2015, **33**, 1141–1161.
29 S. Gupta, M. Hirota, S. M. Waugh, I. Murakami, T. Suzuki, M. Muraguchi, M. Shibamori, Y. Ishikawa, T. C. Jarvis, J. D. Carter, C. Zhang, B. Gawande, M. Vrkljan, N. Janjic and D. J. Schneider, *J. Biol. Chem.*, 2014, **289**, 8706–8719.
30 D. W. Drolet, L. S. Green, L. Gold and N. Janjic, *Nucleic Acid Ther.*, 2016, **26**, 127–146.
31 Y. Chen, Y. Song, Z. He, Z. Wang, W. Liu, F. Wang, X. Zhang and X. Zhou, *Nano Res.*, 2016, **10**, 3084–3092.
32 G. Liang, Y. Man, A. Li, X. Jin, X. Liu and L. Pan, *Microchem. J.*, 2017, **131**, 145–153.
33 M. Liu, Q. Zhang, D. Chang, J. Gu, J. D. Brennan and Y. Li, *Angew. Chem., Int. Ed.*, 2017, **56**, 6142–6146.
34 L. Gong, Z. Zhao, Y.-F. Lv, S.-Y. Huan, T. Fu, X.-B. Zhang, G.-L. Shen and R.-Q. Yu, *Chem. Commun.*, 2015, **51**, 979–995.

35 M. Hollenstein, *Molecules*, 2015, **20**, 20777–20804.

36 S. Wang, L. Yue, Z. Shpilt, A. Cecconello, J. S. Kahn, J.-M. Lehn and I. Willner, *J. Am. Chem. Soc.*, 2017, **139**, 9662–9671.

37 L. Yue, S. Wang, A. Cecconello, J.-M. Lehn and I. Willner, *ACS Nano*, 2017, **11**, 12027–12036.

38 A. Vallée-Bélisle and K. W. Plaxco, *Curr. Opin. Struct. Biol.*, 2010, **20**, 518–526.

39 W. Zhou, P.-J. J. Huang, J. Ding and J. Liu, *Analyst*, 2014, **139**, 2627–2640.

40 A. Vallée-Bélisle, F. Ricci and K. W. Plaxco, *Proc. Natl. Acad. Sci. U. S. A.*, 2009, **106**, 13802–13807.

41 F. Ricci, A. Vallée-Bélisle, A. J. Simon, A. Porchetta and K. W. Plaxco, *Acc. Chem. Res.*, 2016, **49**, 1884–1892.

42 D. D. Boehr, R. Nussinov and P. E. Wright, *Nat. Chem. Biol.*, 2009, **5**, 789–796.

43 J. N. Zadeh, C. D. Steenberg, J. S. Bois, B. R. Wolfe, M. B. Pierce, A. R. Khan, R. M. Dirks and N. A. Pierce, *J. Comput. Chem.*, 2011, **32**, 170–173.

44 M. Zuker, *Nucleic Acids Res.*, 2003, **31**, 3406–3415.

45 B. R. Wolfe, N. J. Porubsky, J. N. Zadeh, R. M. Dirks and N. A. Pierce, *J. Am. Chem. Soc.*, 2017, **139**, 3134–3144.

46 A. Idili, F. Ricci and A. Vallée-Bélisle, *Nucleic Acids Res.*, 2017, **45**, 7571–7580.

47 Y. You, A. V. Tataurov and R. Owczarzy, *Biopolymers*, 2011, **95**, 472–486.

48 S. Tyagi and F. R. Kramer, *Nat. Biotechnol.*, 1996, **14**, 303–308.

49 M. N. Stojanovic, P. De Prada and D. W. Landry, *J. Am. Chem. Soc.*, 2001, **123**, 4928–4931.

50 Z. Tang, P. Mallikaratchy, R. Yang, Y. Kim, Z. Zhu, H. Wang and W. Tan, *J. Am. Chem. Soc.*, 2008, **130**, 11268–11269.

51 R. Nutiu and Y. Li, *J. Am. Chem. Soc.*, 2003, **125**, 4771–4778.

52 D. Y. Zhang and G. Seelig, *Nat. Chem.*, 2011, **3**, 103–113.

53 Y. Xing, Z. Yang and D. Liu, *Angew. Chem., Int. Ed.*, 2011, **50**, 11934–11936.

54 H. Zhang, F. Li, B. Dever, C. Wang, X. F. Li and X. C. Le, *Angew. Chem., Int. Ed.*, 2013, **52**, 10698–10705.

55 W. Tang, H. Wang, D. Wang, Y. Zhao, N. Li and F. Liu, *J. Am. Chem. Soc.*, 2013, **135**, 13628–13631.

56 A. Amodio, B. Zhao, A. Porchetta, A. Idili, M. Castronovo, C. Fan and F. Ricci, *J. Am. Chem. Soc.*, 2014, **136**, 16469–16472.

57 D. Y. Zhang, *J. Am. Chem. Soc.*, 2010, **133**, 1077–1086.

58 X. Chen, *J. Am. Chem. Soc.*, 2011, **134**, 263–271.

59 R. Roy, S. Hohng and T. Ha, *Nat. Methods*, 2008, **5**, 507–516.

60 S. Schlücker, *Angew. Chem., Int. Ed.*, 2014, **53**, 4756–4795.

61 C. Fan, K. W. Plaxco and A. J. Heeger, *Proc. Natl. Acad. Sci. U. S. A.*, 2003, **100**, 9134–9137.

62 J. Kosman and B. Juskowiak, *Anal. Chim. Acta*, 2011, **707**, 7–17.

63 L. Yu, H. Lim, A. Maslova and I. Hsing, *ChemElectroChem*, 2017, **4**, 795–805.

64 E. E. Ferapontova, *Curr. Opin. Electrochem.*, 2017, **5**, 218–225.

65 S. S. Mahshid, S. Camiré, F. Ricci and A. Vallée-Bélisle, *J. Am. Chem. Soc.*, 2015, **137**, 15596–15599.

66 Y. Tang, B. Ge, D. Sen and H.-Z. Yu, *Chem. Soc. Rev.*, 2014, **43**, 518–529.

67 F. Xuan, X. Luo and I. M. Hsing, *Anal. Chem.*, 2013, **85**, 4586–4593.

68 X. Liu, W. Li, T. Hou, S. Dong, G. Yu and F. Li, *Anal. Chem.*, 2015, **87**, 4030–4036.

69 L. Ge, W. Wang, X. Sun, T. Hou and F. Li, *Anal. Chem.*, 2016, **88**, 2212–2219.

70 T. Hou, W. Li, X. Liu and F. Li, *Anal. Chem.*, 2015, **87**, 11368–11374.

71 F. Xuan, T. W. Fan and I. M. Hsing, *ACS Nano*, 2015, **9**, 5027–5033.

72 A. D. Castañeda, N. J. Brenes, A. Kondajji and R. M. Crooks, *J. Am. Chem. Soc.*, 2017, **139**, 7657–7664.

73 C. Feng, S. Dai and L. Wang, *Biosens. Bioelectron.*, 2014, **59**, 64–74.

74 T. Schlichthaerle, M. T. Strauss, F. Schueder, J. B. Woehrstein and R. Jungmann, *Curr. Opin. Biotechnol.*, 2016, **39**, 41–47.

75 J. Huang, X. Yang, X. He, K. Wang, J. Liu, H. Shi, Q. Wang, Q. Guo and D. He, *TrAC, Trends Anal. Chem.*, 2014, **53**, 11–20.

76 Z. Yuan, Y.-C. Chen, H.-W. Li and H.-T. Chang, *Chem. Commun.*, 2014, **50**, 9800–9815.

77 S. Manochehry, M. Liu, D. Chang and Y. Li, *J. Mater. Res.*, 2017, 1–11.

78 M. Liu, W. Zhang, D. Chang, Q. Zhang, J. D. Brennan and Y. Li, *TrAC, Trends Anal. Chem.*, 2015, **74**, 120–129.

79 M. Liu, J. Song, S. Shuang, C. Dong, J. D. Brennan and Y. Li, *ACS Nano*, 2014, **8**, 5564–5573.

80 A.-M. Dallaire, S. Patskovsky, A. Vallée-Bélisle and M. Meunier, *Biosens. Bioelectron.*, 2015, **71**, 75–81.

81 N. H. Kim, S. J. Lee and M. Moskovits, *Nano Lett.*, 2010, **10**, 4181–4185.

82 R. A. Karaballi, A. Nel, S. Krishnan, J. Blackburn and C. L. Brosseau, *Phys. Chem. Chem. Phys.*, 2015, **17**, 21356–21363.

83 A. Barhoumi and N. J. Halas, *J. Am. Chem. Soc.*, 2010, **132**, 12792–12793.

84 I. V. Shevelev and U. Hübscher, *Nat. Rev. Mol. Cell Biol.*, 2002, **3**, 364.

85 X.-H. Zhao, L. Gong, X.-B. Zhang, B. Yang, T. Fu, R. Hu, W. Tan and R. Yu, *Anal. Chem.*, 2013, **85**, 3614–3620.

86 Z. Ge, M. Lin, P. Wang, H. Pei, J. Yan, J. Shi, Q. Huang, D. He, C. Fan and X. Zuo, *Anal. Chem.*, 2014, **86**, 2124–2130.

87 M. M. Ali, F. Li, Z. Zhang, K. Zhang, D.-K. Kang, J. A. Ankrum, X. C. Le and W. Zhao, *Chem. Soc. Rev.*, 2014, **43**, 3324–3341.

88 A. Vallée-Bélisle, F. Ricci and K. W. Plaxco, *J. Am. Chem. Soc.*, 2012, **134**, 2876–2879.

89 J. W. A. Findlay and R. F. Dillard, *AAPS J.*, 2007, **9**, E260–E267.

90 F. Ricci, A. Vallée-Bélisle, A. Porchetta and K. W. Plaxco, *J. Am. Chem. Soc.*, 2012, **134**, 15177–15180.

91 A. J. Simon, A. Vallée-Bélisle, F. Ricci and K. W. Plaxco, *Proc. Natl. Acad. Sci. U. S. A.*, 2014, **111**, 15048–15053.

92 A. J. Simon, A. Vallée-Bélisle, F. Ricci, H. M. Watkins and K. W. Plaxco, *Angew. Chem., Int. Ed.*, 2014, **53**, 9471–9475.

93 H. Prinz, *J. Chem. Biol.*, 2010, **3**, 37–44.

94 A. A. S. T. Ribeiro and V. Ortiz, *Chem. Rev.*, 2016, **116**, 6488–6502.

95 J. Guo and H.-X. Zhou, *Chem. Rev.*, 2016, **116**, 6503–6515.

96 H. N. Motlagh, J. O. Wrabl, J. Li and V. J. Hilser, *Nature*, 2014, **508**, 331–339.

97 R. Nussinov, *Chem. Rev.*, 2016, **116**, 6263–6266.

98 R. A. Laskowski, F. Gerick and J. M. Thornton, *FEBS Lett.*, 2009, **583**, 1692–1698.

99 A. Porchetta, A. Vallée-Bélisle, K. W. Plaxco and F. Ricci, *J. Am. Chem. Soc.*, 2012, **134**, 20601–20604.

100 A. Porchetta, A. Vallée-Bélisle, K. W. Plaxco and F. Ricci, *J. Am. Chem. Soc.*, 2013, **135**, 13238–13241.

101 J. N. Weiss, *FASEB J.*, 1997, **11**, 835–841.

102 D. Mariottini, A. Idili, A. Vallée-Bélisle, K. W. Plaxco and F. Ricci, *Nano Lett.*, 2017, **17**, 3225–3230.

103 A. Porchetta, A. Idili, A. Vallée-Bélisle and F. Ricci, *Nano Lett.*, 2015, **15**, 4467–4471.

104 Y. Ke, T. Meyer, W. M. Shih and G. Bellot, *Nat. Commun.*, 2016, **7**, 10935.

105 K. Furukawa and N. Minakawa, *Org. Biomol. Chem.*, 2014, **12**, 3344–3348.

106 Y. Guo, L. Zhou, L. Xu, X. Zhou, J. Hu and R. Pei, *Sci. Rep.*, 2014, **4**, 7315.

107 E. Agliari, M. Altavilla, A. Barra, L. D. Schiavo and E. Katz, *Sci. Rep.*, 2015, **5**, 9415.

108 F. Ricci, A. Vallée-Bélisle and K. W. Plaxco, *PLoS Comput. Biol.*, 2011, **7**, e1002171.

109 N. E. Buchler and M. Louis, *J. Mol. Biol.*, 2008, **384**, 1106–1119.

110 N. E. Buchler and F. R. Cross, *Mol. Syst. Biol.*, 2009, **5**, 272–272.

111 D. Kang, A. Vallée-Bélisle, A. Porchetta, K. W. Plaxco and F. Ricci, *Angew. Chem., Int. Ed.*, 2012, **51**, 6717–6721.

112 H. Kang, H. Liu, J. A. Phillips, Z. Cao, Y. Kim, Y. Chen, Z. Yang, J. Li and W. Tan, *Nano Lett.*, 2009, **9**, 2690–2696.

113 X. Wang, J. Huang, Y. Zhou, S. Yan, X. Weng, X. Wu, M. Deng and X. Zhou, *Angew. Chem., Int. Ed.*, 2010, **49**, 5305–5309.

114 Y. Yan, X. Wang, J. I. Chen and D. S. Ginger, *J. Am. Chem. Soc.*, 2013, **135**, 8382–8387.

115 F. Wang, X. Liu and I. Willner, *Angew. Chem., Int. Ed.*, 2015, **54**, 1098–1129.

116 J. Zheng, R. Yang, M. Shi, C. Wu, X. Fang, Y. Li, J. Li and W. Tan, *Chem. Soc. Rev.*, 2015, **44**, 3036–3055.

117 S. Song, L. Wang, J. Li, C. Fan and J. Zhao, *TrAC, Trends Anal. Chem.*, 2008, **27**, 108–117.

118 H. Zhang, F. Li, B. Dever, X.-F. Li and X. C. Le, *Chem. Rev.*, 2012, **113**, 2812–2841.

119 R. A. Potyrailo, R. C. Conrad, A. D. Ellington and G. M. Hieftje, *Anal. Chem.*, 1998, **70**, 3419–3425.

120 N. K. Navani and Y. Li, *Curr. Opin. Chem. Biol.*, 2006, **10**, 272–281.

121 I. Willner and M. Zayats, *Angew. Chem., Int. Ed.*, 2007, **46**, 6408–6418.

122 Y. Xu, G. Cheng, P. He and Y. Fang, *Electroanalysis*, 2009, **21**, 1251–1259.

123 A. A. Lubin and K. W. Plaxco, *Acc. Chem. Res.*, 2010, **43**, 496–505.

124 B. Leca-Bouvier and L. J. Blum, *Anal. Lett.*, 2005, **38**, 1491–1517.

125 P. Hong, W. Li and J. Li, *Sensors*, 2012, **12**, 1181–1193.

126 M. McKeague and M. C. DeRosa, *J. Nucleic Acids*, 2012, **2012**, 748913.

127 M. McKeague, A. De Girolamo, S. Valenzano, M. Pascale, A. Ruscito, R. Velu, N. R. Frost, K. Hill, M. Smith, E. M. McConnell and M. C. DeRosa, *Anal. Chem.*, 2015, **87**, 8608–8612.

128 A. Ruscito and M. C. DeRosa, *Front. Chem.*, 2016, **4**, 14.

129 A. Idili, A. Vallée-Bélisle and F. Ricci, *J. Am. Chem. Soc.*, 2014, **136**, 5836–5839.

130 S. Halder and Y. Krishnan, *Nanoscale*, 2015, **7**, 10008–10012.

131 N. Narayanaswamy, R. R. Nair, Y. Suseela, D. K. Saini and T. Govindaraju, *Chem. Commun.*, 2016, **52**, 8741–8744.

132 L. He, D.-Q. Lu, H. Liang, S. Xie, C. Luo, M. Hu, L. Xu, X. Zhang and W. Tan, *ACS Nano*, 2017, **11**, 4060–4066.

133 C. Y. Tay, L. Yuan and D. T. Leong, *ACS Nano*, 2015, **9**, 5609–5617.

134 W. Zhou, D. Li, C. Xiong, R. Yuan and Y. Xiang, *ACS Appl. Mater. Interfaces*, 2016, **8**, 13303–13308.

135 X. Xiao, F.-R. F. Fan, J. Zhou and A. J. Bard, *J. Am. Chem. Soc.*, 2008, **130**, 16669–16677.

136 T. M. Alligrant, E. G. Nettleton and R. M. Crooks, *Lab Chip*, 2013, **13**, 349–354.

137 T. M. Alligrant, R. Dasari, K. J. Stevenson and R. M. Crooks, *Langmuir*, 2015, **31**, 11724–11733.

138 A. D. Castañeda, D. A. Robinson, K. J. Stevenson and R. M. Crooks, *Chem. Sci.*, 2016, **7**, 6450–6457.

139 P. Miao, B. Wang, X. Chen, X. Li and Y. Tang, *ACS Appl. Mater. Interfaces*, 2015, **7**, 6238–6243.

140 J. Jiang, X. Lin and G. Diao, *ACS Appl. Mater. Interfaces*, 2017, **9**, 36688–36694.

141 S. Hu, W. Tang, Y. Zhao, N. Li and F. Liu, *Chem. Sci.*, 2017, **8**, 1021–1026.

142 A. Idili, K. W. Plaxco, A. Vallée-Bélisle and F. Ricci, *ACS Nano*, 2013, **7**, 10863–10869.

143 W. Engelen, K. M. van de Wiel, L. H. Meijer, B. Saha and M. Merkx, *Chem. Commun.*, 2017, **53**, 2862–2865.

144 L. Ge, X. Sun, Q. Hong and F. Li, *ACS Appl. Mater. Interfaces*, 2017, **9**, 13102–13110.

145 S. Bai, T. Wang, Z. Zhang, S. Sheng, W. Yu and G. Xie, *Sens. Actuators, B*, 2017, **239**, 447–454.

146 B. Li, Y. Jiang, X. Chen and A. D. Ellington, *J. Am. Chem. Soc.*, 2012, **134**, 13918–13921.

147 B. Li, A. D. Ellington and X. Chen, *Nucleic Acids Res.*, 2011, **39**, e110–e110.

148 R. M. Dirks and N. A. Pierce, *Proc. Natl. Acad. Sci. U. S. A.*, 2004, **101**, 15275–15278.

149 A. Hayat and J. L. Marty, *Front. Chem.*, 2014, **2**, 41.

150 W. Zhou, R. Saran and J. Liu, *Chem. Rev.*, 2017, **117**, 8272–8325.

151 J. Chen, S. Zhou and J. Wen, *Anal. Chem.*, 2014, **86**, 3108–3114.

152 C.-W. Liu, Y.-T. Hsieh, C.-C. Huang, Z.-H. Lin and H.-T. Chang, *Chem. Commun.*, 2008, 2242–2244.

153 M. Wang, K.-H. Leung, S. Lin, D. S.-H. Chan, C.-H. Leung and D.-L. Ma, *J. Mater. Chem. B*, 2014, **2**, 6467–6471.

154 W. Zhou, J. Ding and J. Liu, *Biosens. Bioelectron.*, 2017, **87**, 171–177.

155 C.-W. Liu, C.-C. Huang and H.-T. Chang, *Anal. Chem.*, 2009, **81**, 2383–2387.

156 S. A. Sander, A. K. Van Hall and J. R. Morrow, *Inorg. Chem.*, 2015, **54**, 3084–3086.

157 W.-Y. Chen, G.-Y. Lan and H.-T. Chang, *Anal. Chem.*, 2011, **83**, 9450–9455.

158 W. Yun, H. Wu, X. Liu, H. Zhong, M. Fu, L. Yang and Y. Huang, *Sens. Actuators, B*, 2018, **255**, 1920–1926.

159 H. Ma, W. Li, W. Zhou and J. Liu, *ChemPlusChem*, 2017, **82**, 1224–1230.

160 B. R. Baker, R. Y. Lai, M. S. Wood, E. H. Doctor, A. J. Heeger and K. W. Plaxco, *J. Am. Chem. Soc.*, 2006, **128**, 3138–3139.

161 M. Zayats, Y. Huang, R. Gill, C.-a. Ma and I. Willner, *J. Am. Chem. Soc.*, 2006, **128**, 13666–13667.

162 W. Zhao, W. Chiuman, J. C. F. Lam, S. A. McManus, W. Chen, Y. Cui, R. Pelton, M. A. Brook and Y. Li, *J. Am. Chem. Soc.*, 2008, **130**, 3610–3618.

163 H. Li, N. y. Arroyo-Currás, D. Kang, F. Ricci and K. W. Plaxco, *J. Am. Chem. Soc.*, 2016, **138**, 15809–15812.

164 B. S. Ferguson, D. A. Hoggarth, D. Maliniak, K. Ploense, R. J. White, N. Woodward, K. Hsieh, A. J. Bonham, M. Eisenstein, T. E. Kippin, K. W. Plaxco and H. T. Soh, *Sci. Transl. Med.*, 2013, **5**, 213ra165–213ra165.

165 H. Li, P. Dauphin-Ducharme, N. Arroyo-Currás, C. H. Tran, P. A. Vieira, S. Li, C. Shin, J. Somerson, T. E. Kippin and K. W. Plaxco, *Angew. Chem., Int. Ed.*, 2017, **56**, 7492–7495.

166 H. Yu, J. Canoura, B. Guntupalli, X. Lou and Y. Xiao, *Chem. Sci.*, 2017, **8**, 131–141.

167 X. Wang, S. Dong, T. Hou, L. Liu, X. Liu and F. Li, *Analyst*, 2016, **141**, 1830–1836.

168 X. Wang, T. Hou, S. Dong, X. Liu and F. Li, *Biosens. Bioelectron.*, 2016, **77**, 644–649.

169 X. Liu, M. Song, T. Hou and F. Li, *ACS Sens.*, 2017, **2**, 562–568.

170 X. Liu, Y. Li, J. Liang, W. Zhu, J. Xu, R. Su, L. Yuan and C. Sun, *Talanta*, 2016, **160**, 99–105.

171 Y. Xiao, B. D. Piorek, K. W. Plaxco and A. J. Heeger, *J. Am. Chem. Soc.*, 2005, **127**, 17990–17991.

172 C.-C. Huang, Y.-F. Huang, Z. Cao, W. Tan and H.-T. Chang, *Anal. Chem.*, 2005, **77**, 5735–5741.

173 S. Ranallo, M. Rossetti, K. W. Plaxco, A. Vallée-Bélisle and F. Ricci, *Angew. Chem.*, 2015, **127**, 13412–13416.

174 A. Vallée-Bélisle, F. Ricci, T. Uzawa, F. Xia and K. W. Plaxco, *J. Am. Chem. Soc.*, 2012, **134**, 15197–15200.

175 A. Vallée-Bélisle, A. J. Bonham, N. O. Reich, F. Ricci and K. W. Plaxco, *J. Am. Chem. Soc.*, 2011, **133**, 13836–13839.

176 L. Xu, W. Yan, W. Ma, H. Kuang, X. Wu, L. Liu, Y. Zhao, L. Wang and C. Xu, *Adv. Mater.*, 2015, **27**, 1706–1711.

177 L. Wei, X. Wang, D. Wu, C. Li, Y. Yin and G. Li, *Chem. Commun.*, 2016, **52**, 5633–5636.

178 S. Su, H. Sun, W. Cao, J. Chao, H. Peng, X. Zuo, L. Yuwen, C. Fan and L. Wang, *ACS Appl. Mater. Interfaces*, 2016, **8**, 6826–6833.

179 M. Ilieva, P. D. Vedova, O. Hansen and M. Dufva, *Front. Cell. Neurosci.*, 2013, **7**, 266.

180 R. Monroy-Contreras and L. Vaca, *J. Nucleic Acids*, 2011, **2011**, 741723.

181 D. A. Giljohann, D. S. Seferos, P. C. Patel, J. E. Millstone, N. L. Rosi and C. A. Mirkin, *Nano Lett.*, 2007, **7**, 3818–3821.

182 A. Giannetti, S. Tombelli and F. Baldini, *Anal. Bioanal. Chem.*, 2013, **405**, 6181–6196.

183 H. Liang, X.-B. Zhang, Y. Lv, L. Gong, R. Wang, X. Zhu, R. Yang and W. Tan, *Acc. Chem. Res.*, 2014, **47**, 1891–1901.

184 N. H. Alami, R. B. Smith, M. A. Carrasco, L. A. Williams, C. S. Winborn, S. S. Han, E. Kiskinis, B. Winborn, B. D. Freibaum, A. Kanagaraj, A. J. Clare, N. M. Badders, B. Bilican, E. Chaum, S. Chandran, C. E. Shaw, K. C. Eggan, T. Maniatis and J. P. Taylor, *Neuron*, 2014, **81**, 536–543.

185 C. Wiraja, D. C. Yeo, M. S. Chong and C. Xu, *Small*, 2016, **12**, 1342–1350.

186 C. Wu, T. Chen, D. Han, M. You, L. Peng, S. Cansiz, G. Zhu, C. Li, X. Xiong, E. Jimenez, C. J. Yang and W. Tan, *ACS Nano*, 2013, **7**, 5724–5731.

187 X. Xiong, Y. Lv, T. Chen, X. Zhang, K. Wang and W. Tan, *Annu. Rev. Anal. Chem.*, 2014, **7**, 405–426.

188 K. Wang, J. Huang, X. Yang, X. He and J. Liu, *Analyst*, 2013, **138**, 62–71.

189 K. Chakraborty, A. T. Veetil, S. R. Jaffrey and Y. Krishnan, *Annu. Rev. Biochem.*, 2016, **85**, 349–373.

190 C. Wiraja, D. Yeo, D. Lio, L. Labanieh, M. Lu, W. Zhao and C. Xu, *Mol. Cell. Ther.*, 2014, **2**, 33.

191 T. Kuang, L. Chang, X. Peng, X. Hu and D. Gallego-Perez, *Trends Biotechnol.*, 2017, **35**, 347–359.

192 R. L. Strack and S. R. Jaffrey, *Curr. Opin. Chem. Biol.*, 2013, **17**, 651–655.

193 J. Ouellet, *Front. Chem.*, 2016, **4**, 29.

194 R. Sandberg, *Nat. Methods*, 2014, **11**, 22–24.

195 D. Longo and J. Hasty, *Mol. Syst. Biol.*, 2006, **2**, 64.

196 K. Lewis, *Annu. Rev. Microbiol.*, 2010, **64**, 357–372.

197 R. Fisher, L. Pusztai and C. Swanton, *Br. J. Cancer*, 2013, **108**, 479–485.

198 M. R. Copley and C. J. Eaves, *Exp. Mol. Med.*, 2013, **45**, e55.

199 Q. F. Wills, K. J. Livak, A. J. Tipping, T. Enver, A. J. Goldson, D. W. Sexton and C. Holmes, *Nat. Biotechnol.*, 2013, **31**, 748–752.

200 K. Ban, B. Wile, K.-W. Cho, S. Kim, M.-K. Song, S. Y. Kim, J. Singer, A. Syed, S. P. Yu, M. Wagner, G. Bao and Y.-s. Yoon, *Stem Cell Rep.*, 2015, **5**, 1239–1249.

201 W. J. Kang, Y. L. Cho, J. R. Chae, J. D. Lee, K.-J. Choi and S. Kim, *Biomaterials*, 2011, **32**, 1915–1922.

202 N. R. Labriola and E. M. Darling, *J. Biomech.*, 2015, **48**, 1058–1066.

203 X.-H. Peng, Z.-H. Cao, J.-T. Xia, G. W. Carlson, M. M. Lewis, W. C. Wood and L. Yang, *Cancer Res.*, 2005, **65**, 1909–1917.

204 C. D. Medley, T. J. Drake, J. M. Tomasini, R. J. Rogers and W. Tan, *Anal. Chem.*, 2005, **77**, 4713–4718.

205 J. S. Paige, K. Y. Wu and S. R. Jaffrey, *Science*, 2011, **333**, 642–646.

206 J. S. Paige, T. Nguyen-Duc, W. Song and S. R. Jaffrey, *Science*, 2012, **335**, 1194–1194.

207 R. L. Strack, W. Song and S. R. Jaffrey, *Nat. Protoc.*, 2014, **9**, 146–155.

208 M. You, J. L. Litke and S. R. Jaffrey, *Proc. Natl. Acad. Sci. U. S. A.*, 2015, **112**, E2756–E2765.

209 W. Song, R. L. Strack and S. R. Jaffrey, *Nat. Methods*, 2013, **10**, 873–875.

210 E. Maisonneuve and K. Gerdes, *Cell*, 2014, **157**, 539–548.

211 S. Modi, M. Swetha, D. Goswami, G. D. Gupta, S. Mayor and Y. Krishnan, *Nat. Nanotechnol.*, 2009, **4**, 325–330.

212 S. Modi, C. Nizak, S. Surana, S. Halder and Y. Krishnan, *Nat. Nanotechnol.*, 2013, **8**, 459–467.

213 R. Deng, L. Tang, Q. Tian, Y. Wang, L. Lin and J. Li, *Angew. Chem., Int. Ed.*, 2014, **53**, 2389–2393.

214 F. R. Maxfield, *Cold Spring Harbor Perspect. Biol.*, 2014, **6**, a016931.

215 D. Y. Vargas, A. Raj, S. A. Marras, F. R. Kramer and S. Tyagi, *Proc. Natl. Acad. Sci. U. S. A.*, 2005, **102**, 17008–17013.

216 D. Zhao, Y. Yang, N. Qu, M. Chen, Z. Ma, C. J. Krueger, M. A. Behlke and A. K. Chen, *Biomaterials*, 2016, **100**, 172–183.

217 J. Zhang, J. Fei, B. J. Leslie, K. Y. Han, T. E. Kuhlman and T. Ha, *Sci. Rep.*, 2015, **5**, 17295.

218 S. Tyagi, *Nat. Methods*, 2009, **6**, 331–338.

219 B. Koos, G. Cane, K. Grannas, L. Löf, L. Arngården, J. Heldin, C.-M. Clausson, A. Klaesson, M. K. Hirvonen, F. M. De Oliveira, V. O. Talibov, N. T. Pham, M. Auer, U. H. Danielson, J. Haybaeck, M. Kamali-Moghaddam and O. Söderberg, *Nat. Commun.*, 2015, **6**, 7294.

220 C.-M. Clausson, *PhD*, Uppsala University, 2014.

221 M. E. Tanenbaum, L. A. Gilbert, L. S. Qi, J. S. Weissman and R. D. Vale, *Cell*, 2014, **159**, 635–646.

222 O. Söderberg, M. Gullberg, M. Jarvius, K. Ridderstråle, K.-J. Leuchowius, J. Jarvius, K. Wester, P. Hydbring, F. Bahram, L.-G. Larsson and U. Landegren, *Nat. Methods*, 2006, **3**, 995–1000.

223 M. You, Y. Lyu, D. Han, L. Qiu, Q. Liu, T. Chen, C. S. Wu, L. Peng, L. Zhang, G. Bao and W. Tan, *Nat. Nanotechnol.*, 2017, **12**, 453–459.

224 P. A. Beales, *Nat. Nanotechnol.*, 2017, **12**, 404–406.

225 Y. Zhang, C. Ge, C. Zhu and K. Salaita, *Nat. Commun.*, 2014, **5**, 5167.

226 W. Zhao, S. Schafer, J. Choi, Y. J. Yamanaka, M. L. Lombardi, S. Bose, A. L. Carlson, J. A. Phillips, W. Teo, I. A. Droujinine, C. H. Cui, R. K. Jain, J. Lammerding, J. C. Love, C. P. Lin, D. Sarkar, R. Karnik and J. M. Karp, *Nat. Nanotechnol.*, 2011, **6**, 524–531.

227 L. Qiu, T. Zhang, J. Jiang, C. Wu, G. Zhu, M. You, X. Chen, L. Zhang, C. Cui, R. Yu and W. Tan, *J. Am. Chem. Soc.*, 2014, **136**, 13090–13093.

228 M. Xiong, H. Zhu, Q. Rong, C. Yang, L. Qiu, X.-B. Zhang and W. Tan, *Chem. Commun.*, 2016, **52**, 4679–4682.

229 M. M. Ali, D. K. Kang, K. Tsang, M. Fu, J. M. Karp and W. Zhao, *Wiley Interdiscip. Rev.: Nanomed. Nanobiotechnol.*, 2012, **4**, 547–561.

230 K. Engin, D. Leeper, J. Cater, A. Thistlethwaite, L. Tupchong and J. McFarlane, *Int. J. Hyperthermia*, 1995, **11**, 211–216.

231 M. Stubbs, P. M. McSheehy, J. R. Griffiths and C. L. Bashford, *Mol. Med. Today*, 2000, **6**, 15–19.

232 E. Del Grosso, A.-M. Dallaire, A. Vallée-Bélisle and F. Ricci, *Nano Lett.*, 2015, **15**, 8407–8411.

233 S. Ranallo, C. Prévost-Tremblay, A. Idili, A. Vallée-Bélisle and F. Ricci, *Nat. Commun.*, 2017, **8**, 15150.

234 E. McConnell, R. Bolzon, P. Mezin, G. Frahm, M. Johnston and M. DeRosa, *Bioconjugate Chem.*, 2016, **27**, 1493–1499.

235 C. E. Castro, F. Kilchherr, D.-N. Kim, E. L. Shiao, T. Wauer, P. Wortmann, M. Bathe and H. Dietz, *Nat. Methods*, 2011, **8**, 221–229.

236 T. Tørring, N. V. Voigt, J. Nangreave, H. Yan and K. V. Gothelf, *Chem. Soc. Rev.*, 2011, **40**, 5636–5646.

237 J. Nangreave, D. Han, Y. Liu and H. Yan, *Curr. Opin. Chem. Biol.*, 2010, **14**, 608–615.

238 E. S. Andersen, M. Dong, M. M. Nielsen, K. Jahn, R. Subramani, W. Mamdouh, M. M. Golas, B. Sander, H. Stark, C. L. Oliveira, J. S. Pedersen, V. Birkedal, F. Besenbacher, K. V. Gothelf and J. Kjems, *Nature*, 2009, **459**, 73–76.

239 A. Banerjee, D. Bhatia, A. Saminathan, S. Chakraborty, S. Kar and Y. Krishnan, *Angew. Chem., Int. Ed.*, 2013, **52**, 6854–6857.

240 D. Bhatia, S. Surana, S. Chakraborty, S. P. Koushika and Y. Krishnan, *Nat. Commun.*, 2011, **2**, 339.

241 T. G. Edwardson, K. M. Carneiro, C. K. McLaughlin, C. J. Serpell and H. F. Sleiman, *Nat. Chem.*, 2013, **5**, 868–875.

242 P. Chidchob, T. G. Edwardson, C. J. Serpell and H. F. Sleiman, *J. Am. Chem. Soc.*, 2016, **138**, 4416–4425.

243 P. K. Lo, P. Karam, F. A. Aldaye, C. K. McLaughlin, G. D. Hamblin, G. Cosa and H. F. Sleiman, *Nat. Chem.*, 2010, **2**, 319–328.

244 S. M. Douglas, I. Bachelet and G. M. Church, *Science*, 2012, **335**, 831–834.

245 E. Ruiz-Hernandez, A. Baeza and M. Vallet-Regí, *ACS Nano*, 2011, **5**, 1259–1266.

246 W.-C. Liao, C.-H. Lu, R. Hartmann, F. Wang, Y. S. Sohn, W. J. Parak and I. Willner, *ACS Nano*, 2015, **9**, 9078–9086.

247 K. E. Bujold, J. Fakhoury, T. G. Edwardson, K. M. Carneiro, J. N. Briard, A. G. Godin, L. Amrein, G. D. Hamblin, L. C. Panasci, P. W. Wiseman and H. F. Sleiman, *Chem. Sci.*, 2014, **5**, 2449–2455.

248 W. C. Liao and I. Willner, *Adv. Funct. Mater.*, 2017, **27**, 1702732.

249 W.-C. Liao, M. Riutin, W. J. Parak and I. Willner, *ACS Nano*, 2016, **10**, 8683–8689.

250 Z. Xiao, C. Ji, J. Shi, E. M. Pridgen, J. Frieder, J. Wu and O. C. Farokhzad, *Angew. Chem.*, 2012, **124**, 12023–12027.

251 P. Zhang, C. Wang, J. Zhao, A. Xiao, Q. Shen, L. Li, J. Li, J. Zhang, Q. Min, J. Chen, H.-Y. Chen and J.-J. Zhu, *ACS Nano*, 2016, **10**, 3637–3647.

252 J. S. Kahn, L. Freage, N. Enkin, M. A. A. Garcia and I. Willner, *Adv. Mater.*, 2017, **29**, 1602782.

253 L. Song, V. H. Ho, C. Chen, Z. Yang, D. Liu, R. Chen and D. Zhou, *Adv. Healthcare Mater.*, 2013, **2**, 275–280.

254 D. Wang, Y. Zhang and D. Liu, *F1000Research*, 2017, **6**, 503.

255 X. Hou, W. Guo, F. Xia, F.-Q. Nie, H. Dong, Y. Tian, L. Wen, L. Wang, L. Cao, Y. Yang, J. Xue, Y. Song, Y. Wang, D. Liu and L. Jiang, *J. Am. Chem. Soc.*, 2009, **131**, 7800–7805.

256 P. Li, G. Xie, X. Y. Kong, Z. Zhang, K. Xiao, L. Wen and L. Jiang, *Angew. Chem., Int. Ed.*, 2016, **55**, 15637–15641.

257 J. R. Burns, A. Seifert, N. Fertig and S. Howorka, *Nat. Nanotechnol.*, 2016, **11**, 152–156.

258 D. Wang, Y. Zhang, M. Wang, Y. Dong, C. Zhou, M. A. Isbell, Z. Yang, H. Liu and D. Liu, *Nanoscale*, 2016, **8**, 3944–3948.

259 X. Xiong, C. Wu, C. Zhou, G. Zhu, Z. Chen and W. Tan, *Macromol. Rapid Commun.*, 2013, **34**, 1271–1283.

260 J. S. Kahn, Y. Hu and I. Willner, *Acc. Chem. Res.*, 2017, **50**, 680–690.

261 D. Liu, E. Cheng and Z. Yang, *NPG Asia Mater.*, 2011, **3**, 109.

262 E. Mastronardi, A. Foster, X. Zhang and M. C. DeRosa, *Sensors*, 2014, **14**, 3156–3171.

263 L. Peng, M. You, Q. Yuan, C. Wu, D. Han, Y. Chen, Z. Zhong, J. Xue and W. Tan, *J. Am. Chem. Soc.*, 2012, **134**, 12302–12307.

264 Y. Hu, C. H. Lu, W. Guo, M. A. Aleman-Garcia, J. Ren and I. Willner, *Adv. Funct. Mater.*, 2015, **25**, 6867–6874.

265 W. Guo, C. H. Lu, R. Orbach, F. Wang, X. J. Qi, A. Cecconello, D. Seliktar and I. Willner, *Adv. Mater.*, 2015, **27**, 73–78.

266 C.-H. Lu, W. Guo, Y. Hu, X.-J. Qi and I. Willner, *J. Am. Chem. Soc.*, 2015, **137**, 15723–15731.

267 X. Yu, Y. Hu, J. S. Kahn, A. Cecconello and I. Willner, *Chem. – Eur. J.*, 2016, **22**, 14504–14507.

268 Y. Hu, J. S. Kahn, W. Guo, F. Huang, M. Fadeev, D. Harries and I. Willner, *J. Am. Chem. Soc.*, 2016, **138**, 16112–16119.

269 L. Zhang, J. Lei, L. Liu, C. Li and H. Ju, *Anal. Chem.*, 2013, **85**, 11077–11082.

270 H. Kang, H. Liu, X. Zhang, J. Yan, Z. Zhu, L. Peng, H. Yang, Y. Kim and W. Tan, *Langmuir*, 2010, **27**, 399–408.

271 J. Song, S. Hwang, K. Im, J. Hur, J. Nam, S. Hwang, G.-O. Ahn, S. Kim and N. Park, *J. Mater. Chem. B*, 2015, **3**, 1537–1543.

272 Y. Li, Y. Liu, R. Ma, Y. Xu, Y. Zhang, B. Li, Y. An and L. Shi, *ACS Appl. Mater. Interfaces*, 2017, **9**, 13056–13067.

273 J. Pan, F. Li, T.-G. Cha, H. Chen and J. H. Choi, *Curr. Opin. Biotechnol.*, 2015, **34**, 56–64.

274 J. Bath and A. J. Turberfield, *Nat. Nanotechnol.*, 2007, **2**, 275–284.

275 S. Kassem, T. van Leeuwen, A. S. Lubbe, M. R. Wilson, B. L. Feringa and D. A. Leigh, *Chem. Soc. Rev.*, 2017, **46**, 2592–2621.

276 X. Qu, D. Zhu, G. Yao, S. Su, J. Chao, H. Liu, X. Zuo, L. Wang, J. Shi, L. Wang, W. Huang, H. Pei and C. Fan, *Angew. Chem., Int. Ed.*, 2017, **56**, 1855–1858.

277 X. Yang, Y. Tang, S. D. Mason, J. Chen and F. Li, *ACS Nano*, 2016, **10**, 2324–2330.

278 Y. He and D. R. Liu, *Nat. Nanotechnol.*, 2010, **5**, 778–782.

279 M. You, Y. Chen, X. Zhang, H. Liu, R. Wang, K. Wang, K. R. Williams and W. Tan, *Angew. Chem.*, 2012, **124**, 2507–2510.

280 Z.-G. Wang, J. Elbaz and I. Willner, *Nano Lett.*, 2010, **11**, 304–309.

281 K. Lund, A. J. Manzo, N. Dabby, N. Michelotti, A. Johnson-Buck, J. Nangreave, S. Taylor, R. Pei, M. N. Stojanovic, N. G. Walter, E. Winfree and H. Yan, *Nature*, 2010, **465**, 206–210.

282 W. Li, L. Wang and W. Jiang, *Chem. Commun.*, 2017, **53**, 5527–5530.

283 E. Katz, *Curr. Opin. Biotechnol.*, 2015, **34**, 202–208.

284 L. Adleman, *Science*, 1994, **266**, 1021–1024.

285 E. Winfree, F. Liu, L. A. Wenzler and N. C. Seeman, *Nature*, 1998, **394**, 539–544.

286 R. Pei, E. Matamoros, M. Liu, D. Stefanovic and M. N. Stojanovic, *Nat. Nanotechnol.*, 2010, **5**, 773–777.

287 J. Macdonald, Y. Li, M. Sutovic, H. Lederman, K. Pendri, W. Lu, B. L. Andrews, D. Stefanovic and M. N. Stojanovic, *Nano Lett.*, 2006, **6**, 2598–2603.

288 M. N. Stojanovic and D. Stefanovic, *Nat. Biotechnol.*, 2003, **21**, 1069–1074.

289 M. N. Stojanovic, D. Stefanovic and S. Rudchenko, *Acc. Chem. Res.*, 2014, **47**, 1845–1852.

290 L. Qian and E. Winfree, *Science*, 2011, **332**, 1196–1201.

291 J. Chen, S. Zhou and J. Wen, *Angew. Chem., Int. Ed.*, 2015, **54**, 446–450.

292 M. You, G. Zhu, T. Chen, M. J. Donovan and W. Tan, *J. Am. Chem. Soc.*, 2015, **137**, 667–674.

293 M. You, L. Peng, N. Shao, L. Zhang, L. Qiu, C. Cui and W. Tan, *J. Am. Chem. Soc.*, 2014, **136**, 1256–1259.

294 D. Han, G. Zhu, C. Wu, Z. Zhu, T. Chen, X. Zhang and W. Tan, *ACS Nano*, 2013, **7**, 2312–2319.

295 L. Feng, Z. Lyu, A. Offenhäusser and D. Mayer, *Angew. Chem., Int. Ed.*, 2015, **54**, 7693–7697.

296 L. Ge, W. Wang, X. Sun, T. Hou and F. Li, *Anal. Chem.*, 2016, **88**, 9691–9698.

297 X. Liu, R. Aizen, R. Freeman, O. Yehezkeli and I. Willner, *ACS Nano*, 2012, **6**, 3553–3563.

298 B. M. G. Janssen, E. H. M. Lempens, L. L. C. Olijve, I. K. Voets, J. L. J. van Dongen, T. F. A. de Greef and M. Merkx, *Chem. Sci.*, 2013, **4**, 1442–1450.

299 B. M. G. Janssen, M. van Rosmalen, L. van Beek and M. Merkx, *Angew. Chem.*, 2015, **127**, 2560–2563.

300 S. Mailloux, Y. V. Gerasimova, N. Guz, D. M. Kolpashchikov and E. Katz, *Angew. Chem., Int. Ed.*, 2015, **54**, 6562–6566.

301 S. K. Silverman, *Angew. Chem., Int. Ed.*, 2010, **49**, 7180–7201.

302 D. Coquière, B. L. Feringa and G. Roelfes, *Angew. Chem.*, 2007, **119**, 9468–9471.

303 J. Oelerich and G. Roelfes, *Chem. Sci.*, 2013, **4**, 2013–2017.

304 A. J. Boersma, B. L. Feringa and G. Roelfes, *Org. Lett.*, 2007, **9**, 3647–3650.

305 C. Wang, G. Jia, J. Zhou, Y. Li, Y. Liu, S. Lu and C. Li, *Angew. Chem., Int. Ed.*, 2012, **51**, 9352–9355.

306 Y. Chen and C. Mao, *J. Am. Chem. Soc.*, 2004, **126**, 13240–13241.

307 T. R. Fadel, D. F. Farrell, L. E. Friedersdorf, M. H. Griep, M. D. Hoover, M. A. Meador and M. Meyyappan, *ACS Sens.*, 2016, **1**, 207–216.

308 S. Bamrungsap, Z. Zhao, T. Chen, L. Wang, C. Li, T. Fu and W. Tan, *Nanomedicine*, 2012, **7**, 1253–1271.

309 T. Tørring and K. V. Gothelf, *F1000Prime Rep.*, 2013, **5**, 14.